8-10-2018

Examining the Effects of Directional Wave Spectra on a Nearshore Wave Model

Sally Catherine Davis Dillon

Examining the effects of directional wave spectra on a nearshore wave model

By

Sally Catherine Davis Dillon

A Thesis
Submitted to the Faculty of
Mississippi State University
in Partial Fulfillment of the Requirements
for the Degree of Master of Science
in Biological Engineering
in the Department of Agricultural and Biological Engineering

Mississippi State, Mississippi

August 2018

Examining the effects of directional wave spectra on a nearshore wave model

By

Sally Catherine Davis Dillon

Approved:

_____

Anna C. Linhoss
(Major Professor)

_____

Adam Skarke
(Committee Member)

_____

Jane M. Smith
(Committee Member)

_____

Fei Yu
(Graduate Coordinator)

_____

Jason Keith
Dean
Bagley College of Engineering

Name: Sally Catherine Davis Dillon

Date of Degree: August 10, 2018

Institution: Mississippi State University

Major Field: Biological Engineering

Major Professor: Anna C. Linhoss

Title of Study: Examining the effects of directional wave spectra on a nearshore wave model

Pages in Study 73

Candidate for Degree of Master of Science

Wave models are an integral part of coastal engineering due to their ability to quantify information that is either unobtainable or unavailable. However, these models rely heavily on their directional wave spectrum inputs which describe the variation of energy in frequency and direction. This study investigated how five methods for computing the directional wave spectrum perform within the nearshore wave model, STWAVE. The results of the five runs showed that overall, the greatest differences between spectra were observed in the significant wave height parameter. The mean wave direction showed greater differences at the offshore model domain boundary and lesser differences as the wave enters the nearshore; and the peak period had fewer differences at the boundary, but at the nearshore the differences were dependent upon the presence of wind forcing. Winds had a significant impact on observed differences between the spectra in the domain by dominating the wave field variation.

DEDICATION

I would like to dedicate this research to my husband, Devin, and my parents, Jack and Mimi.

ACKNOWLEDGEMENTS

Sincere thanks are due to Dr. Anna Linhoss, my major professor, for her support, and encouragement throughout this processes. I also would like to thank Dr. Robert Jensen, Dr. Jane Smith, and Mary Bryant from the U.S. Army Engineer Research and Development Center, for their expertise, aid, and guidance.

TABLE OF CONTENTS

LIST OF TABLES

LIST OF FIGURES

CHAPTER I

BACKGROUND

Waves drive the natural processes of the coast. When these processes threaten infrastructure, property, or lives, engineering techniques and structures become necessary to reduce those risks. However, before any designs or techniques can be implemented, the wave environment must be understood and accurately characterized. To better understand coastal wave conditions, nearshore transformation models are often used due to their ease of implementation and efficiency. Nearshore transformation models simulate the transformation of offshore waves into the nearshore focusing on the dominant processes of wave shoaling, wave refraction, sheltering, and depth-induced wave breaking. To simulate the wave environment within the wave model, a directional wave spectrum is used as the initial forcing condition (Panicker and Borgman 1970).

A directional wave spectrum is the conceptual interpretation of a sea state used to quantify it for an interval of time. The directional spectrum is created by transforming a frequency spectrum with a directional spreading function, which spreads the energy density about the mean wave direction. This is expressed as:

$$S(f,\theta)=E(f)D(\theta,f) \tag{1.1}$$

Where, $S(f,\theta)$, (m^2/Hz/deg) is the directional spectrum, $E(f)$, (m^2/Hz) is the frequency spectrum (energy density), $D(\theta,f)$ (Hz/deg) is the directional spread function.

There are multiple methods for computing a directional wave spectrum and multiple parameterizations for estimating the frequency spectral shape and the spreading function. The choice of calculation method is typically dependent upon the available information. If there is an offshore buoy, then a Fast Fourier Transformation (FFT) is applied to estimate a frequency spectrum from the measured heave acceleration of the buoy. A frequency spectrum differentiates each wave based on its period and creates a one-dimensional spectrum correlating wave energy with each frequency. The FFT method used to derive frequency spectra using the time series of the heave of a buoy is described in detail by Steele et al. (1992) in an NDBC briefing. The FFT technique is expressed as:

$$S_w(f) = \frac{S_h(f)}{PTF} \tag{1.2}$$

Where, $S_h(f)$ is a spectrum of buoy heave motion, PTF is a power transfer function, and $S_w(f)$ is the wave spectrum first described as acceleration and then transformed into displacement, which creates the frequency spectrum.

Given directional capabilities, a buoy is also able to calculate co- and quad-spectra coefficients from the pitch and roll of the buoy (Longuet-Higgins et al. 1963; Earle 1996; Steele et al. 1992). These coefficients are used to estimate directional spreading. The directional spreading functions indicate how much of the given energy density in the frequency spectrum is spread over each direction for each frequency band. Usually, the first and second Fourier transformation coefficients, r_1 and r_2, which describe directional energy spreading, and the third and fourth coefficients, α_1 and α_2, which describe the mean and principal wave direction (Earle 1996) are used. Discussed below

are three common methods to estimate direction spreading using the FFT directional coefficients.

The first method is the Longuet-Higgins spreading function (LH) described by Longuet-Higgins et al. (1963) and Brissette et al. (1994) and also referred to as the Direct Spectral Method by Goda (1985). This function produces broad peaks with energy being symmetrically distributed around the mean wave direction. The function is described as:

$$D(f,\theta) = \frac{1}{\pi}[\frac{1}{2} + r_1 \cos(a - \alpha_1) + r_2 \cos\big(2(a - \alpha_2)\big)] \quad (1.3)$$

where, r_1 and r_2 are the first and second Fourier transformation coefficients and describe directional energy spreading, and α_1 and α_2 are the third and fourth coefficients and describe the mean and principal wave direction (Earle 1996).

The Maximum Likelihood Method (MLM) defined by Capon (1969), Brissette et al. (1994), Waals et al. (2002), and Memos and Tsiachris (2001) is another method that uses FFT directional coefficients. This method estimates the mean and variance for the directional spectrum, and then creates a distribution with those parameters (Capon 1969). The maximum likelihood method is described as:

$$D(f,\theta) = \frac{1}{2}a_0 + a1\cos(\theta) + b_1 \sin(\theta) + a_2 \cos(2\theta) + b_2 \sin(2\theta) \quad (1.4)$$

where a_0, a_1, b_1, a_2, and b_2 are computed using the cross spectral densities utilizing the r_1, r_2, α_1, α_2, and frequency spectral values.

The Maximum Entropy Method (MEM) described by Lygre and Krogstad (1986), Hashimoto et al. (1995), Brissette et al. (1994), Nwogu (1989), and Memos and Tsiachris (2001) estimates the distribution with the highest entropy. It is computed using the cross

spectral density matrix obtained by the FFT to estimate the directional spread for each frequency band (Lygre and Krogstad 1986), and is expressed as:

$$D(f,\theta) = \frac{1-d_1c_1-d_2c_2}{2\pi\left|1-d_1e^{-i\varphi}-d_2e^{-2i\varphi}\right|^2} \quad (1.5)$$

where, d_1, d_2, c_1, and c_2 are computed using the cross spectral densities utilizing the r_1, r_2, α_1, α_2, and frequency spectral values.

If there is no measurement information to produce a frequency spectra and/or directional coefficients, then a standard parametric spectral shape can be used based on wave parameters. The Pierson-Moskowitz spectrum is an empirical relationship that creates a frequency spectrum through the distribution of energy over frequencies. This method is one of the simplest methods and assumes fully developed seas or that waves are as large as they can grow for a given wind speed (Pierson & Moskowitz 1964). An extension of the Pierson-Moskowitz spectrum was parameterized from measurements taken during the Joint North Sea Wave Project (JONSWAP). The JONSWAP spectrum is an empirical relationship that defines how energy is distributed with frequency. This method was developed for fetch-limited waves, the most common limit on wave growth, with total energy specified by an alpha term. The peakedness is specified by a gamma term (γ), and the asymmetry of the energy is distributed around the peak frequency determined by σ_a and σ_b (Hasselmann et al. 1973; Bouws et al. 1985; Kitaigordskii et al. 1975; Goda 1999). The JONSWAP spectrum is parameterized by the significant wave height, peak period, and mean wave direction and is defined as:

$$(f) = \frac{\alpha g^2}{(2\pi)^4 f^5} e^{-1.25\left(\frac{f_p}{f}\right)^4} y^{\alpha} \quad (1.6)$$

Where, $\alpha = e^{-\left[\frac{(f-f_p)^2}{2\sigma^2 f_p^2}\right]}$, γ= 3.3, σ_a = 0.07 when $f < f_p$ and σ_b = 0.09 when $f \geq f_p$ (Sorensen 2005).

The JONSWAP frequency spectrum has some limitations as it is an approximation of the frequency spectrum, includes a single wave train and distributes energy parametrically about the peak frequency.

Without directional information, the cosine squared (Cos^2) or cosine 2s (Cos^{2s}) spreading functions can be used (Kumar et al. 2000; Hughes 1985, Long 1980) to estimate directional spreading. The Cos^2 function uses the cosine squared shape and applies it to all frequency bands. This is defined as:

$$D(f,\theta) = \cos^2(\theta - \theta_m) \tag{1.7}$$

where, θ_m is the mean wave direction and D(f,θ) = 0, when $|\theta - \theta_m| > \frac{\pi}{2}$, so the energy is spread only ±90 degrees about the mean wave direction.

The Cos^{2s} function also uses the cosine squared-based shape applied to all frequency bands but includes a spreading parameter "s", which narrows the shape of the spreading (Hughes 1985). This changes the directional spread expression to:

$$D(f,\theta) = G(s)\cos^{2s}(\frac{\theta-\theta_m}{2}) \tag{1.8}$$

where, $G(s) = 0.5\sqrt{\pi} * \frac{\Gamma(s+1)}{\Gamma(s+0.5)}$, $s = \frac{r_1}{1-r_1}$, and r_1 is the first FFT coefficient.

Goda (1999), Earle et al. (1999), and Brissette et al. (1994) discussed the differences between these formulations, however, less is known about the impact these different formulations have when applied within a spectral wave model. Earle et al. (1999) briefly concluded that which method is best to use with a spectral wave model is

not documented and should be determined based on the intended application. He also stated that while each method has advantages and disadvantages, it is unknown whether these affect the application and is hard to conclude which to use *a priori*. Therefore, due to the common application of nearshore wave models and the importance of the spectra used to force the models, this study investigates how different computations of directional wave spectra used as input at the wave model boundary affect the outputs of a nearshore wave model.

CHAPTER II

STUDY SITE

Figure 2.1 Study site location with model grid domain and location of offshore buoy

The study site is the Northern Gulf of Mexico around the Mississippi Sound (Figure 2.1). The area has been modeled extensively by the spectral wave models, WAM, WAVEWATCH III, SWAN, and STWAVE (alone, nested, and coupled) by Ahsan et al. (2002, 2002), Blumberg et al. (2000), Wamsley et al. (2013), Bunya et al. (2010), Smith (2007), Jensen (1983), Sheng and Butler (1982), and Hsu et al. (2000) for projects related to the high occurrence of hurricanes and the need for beach re-nourishment. The Mississippi Sound under average conditions is best described as shallow, sheltered, and low energy. The area is about six times longer (east to west) than it is wide (south to north) and is sheltered by five barrier islands. The average depth is 4 m with two shipping channels running north to south at Gulfport and Pascagoula/Bayou Casotte (Outlaw 1983). The area is on the inner continental shelf with bottom sediments mainly comprised of sand or a sand and mud mixture (Veeramoney et al. 2014; Blumberg et al. 2000). The average wave conditions are fetch limited with wave heights less than a meter and periods of 3 seconds or less (Outlaw 1983).

To characterize the offshore waves in this location, Station 42040 from the National Oceanic and Atmospheric Administration's National Data Buoy Center (NDBC) was used. The buoy was located 63 nautical miles (nm) south of Dauphin Island, Alabama, at 29.2-degrees North and 88.2-degrees West. The buoy was moored at a water depth of 237 m. The buoy data provides frequency spectra and directional coefficients generated from a Fast Fourier Transformation (FFT) of the buoy's motion as well as significant wave height, peak period, and mean wave direction, recorded hourly.

The time frame used in the study to simulate waves was September 16-18, 2016. This time period coincided with the deployment of a nearshore Nortek PUV wave gauge

and with favorable onshore weather conditions (i.e. no alongshore storms). The Nortek PUV wave gauge was deployed half a mile off the shore of Deer Island, Biloxi, MS (30.22 N and 88.53 W), and moored at an approximate depth of 2 m. In the future, the PUV wave gauge will be used to help determine the most appropriate directional wave spectra shape for the area and validate modeling.

For this time period, the wave heights at the offshore buoy ranged from 0.4 m to 0.7 m with an average wave direction of 90 degrees and the most predominant wave direction was 112 degrees. Directions are measured in the meteorological convention, where 0 degrees is a wave headed towards the south (or from the north). The peak period ranged from 3.8 seconds to 5.5 seconds with an average of 4.7 seconds and the most common being 4.5 seconds. The most common winds measured from the offshore buoy used an anemometer set 4 m above the site elevation. The prevailing wind direction for the time period was approximately 160 degrees or headed toward the northwest. The maximum wind speed was 7.7 m/s from 163 degrees or west and the minimum wind speed was 1.5 m/s from 169 degrees or west.

CHAPTER III

PROCEDURE

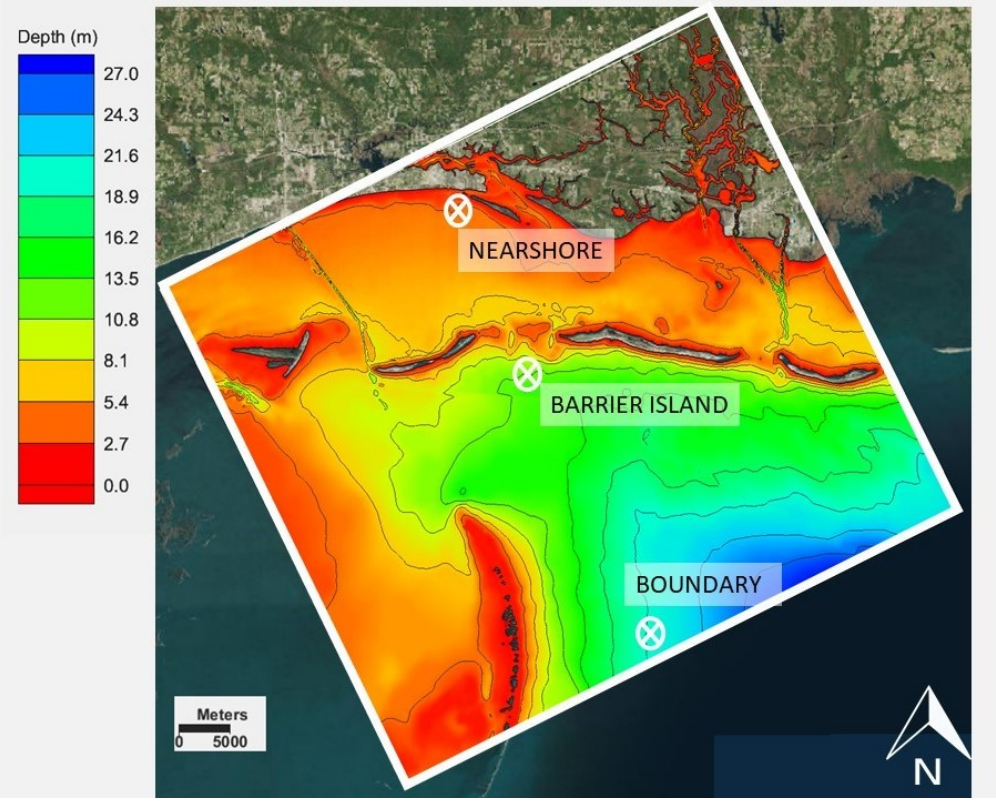

Figure 3.1 Bathymetric grid showing the depth contours of the area, as well as the location of the three selected output points.

To investigate the effects of different parameterizations of directional wave spectra on wave model outputs, five different types of directional wave spectra were generated based on the NDBC buoy measurement to drive the wave model at the offshore

boundary. Three of the spectra types were created using the buoy generated FFT frequency spectra with LH, MLM, and MEM spreading functions applied. The other two directional wave spectra were created using JONSWAP frequency spectra and the $\cos^2$ and $\cos^{2s}$ spreading functions. These methods were chosen because the first three rely on measured data which are more precise and the last two rely on approximations generated by averages produced by measured data. The JONSWAP frequency spectrum was chosen over the Pierson-Moskowitz frequency spectra because of its fetch-limited assumption and ability to represent fetch-limited waves.

After the input spectra were created, STWAVE (Smith et al. 2001, Massey et al. 2011), a nearshore spectral wave model, was run for 71 cases, September 16, 2016 00:40 to September 18, 2016 23:40 in one-hour time increments. Within the STWAVE model grid, three stations at key wave transformation locations were selected to output wave parameter data (wave height, peak period, and mean direction). These points were along the boundary, Gulf-ward of the barrier islands, and in the sheltered nearshore (Figure 3.1). These points are located 85 km, 115 km, and 135 km respectively from the offshore buoy. STWAVE was run without tides or wind, with tides, and with winds to investigate how these conditions affect the wave parameter outputs of each spectrum within the model. Differences in wave parameter outputs were expected between each spectral input type, because although the inputs for all five directional wave spectra were generated from the same buoy data, the spectra varies due to the differences in frequency and directional distribution of energy. This study analyzed the effect these differences in energy distribution have on STWAVE outputs.

3.1 Nearshore Wave Model

STWAVE (Smith et al. 2001, Massey et al. 2011) is a stationary, finite difference, phase averaging, spectral wave model based on the wave action balance equation, which is able to quantitatively describe changes that are due to the influence of bathymetry, currents, and water level on wave parameters as waves move towards shore. STWAVE simulates wave-bottom interactions, the influence of currents, growth due to winds, refraction, shoaling, and breaking and the corresponding changes to wave energy.

The half-plane version of STWAVE, was used to investigate the five different directional spectral computations. The half-plane mode allows wave energy to propagate from offshore towards shore within ± 85-degrees from the x-axis, ignoring all waves traveling in a negative x direction (i.e., wave reflection or offshore wave growth). Only wave transformation and generation processes as the waves propagate towards the shore are included. The wind and wave inputs and outputs are measured in degrees counterclockwise from the grid's x-axis. The grid is oriented with its x-axis aligned across-shore at 116 degrees, and with the y-axis aligned along-shore at ±85 degrees about the x-axis (31 degrees to 201 degrees).

3.1.1 Wave Model Simulation Inputs

The inputs to STWAVE include 1) a bathymetry grid, 2) wind speeds and directions, 3) bottom friction specified over the entire grid, and 4) the directional wave spectra input at the offshore grid boundary. The bathymetry grid was taken from an Advanced Circulation Model (ADCIRC) grid, with a NAD 27 horizontal datum and NAD 83 vertical datum. The gird was 62.3 kilometers by 69.6 kilometers with square grid cells and a grid spacing of 100 m (Figure 2.1). The grid's azimuth was116-degrees,

measured in the polar coordinate system (east is 0 degrees). The azimuth is the rotation of the model grid counterclockwise from the east, reported in degrees. Due to the distance of the buoy from the shore and the high-frequency wave climate of the area, wave transformation does not occur until the depth of the water is less than around 25-27 m during the selected time period. So, to include a higher grid resolution without decreasing the model's efficiency (grid size), the bathymetry grid was shortened approximately 85 kilometers to the area inshore of the approximate 27-m depth contour.

The directional wave spectra input was computed using the buoy data. The buoy provided frequency spectra calculated using an FFT of the buoy's heave, the buoy up and down motion, and the energy is placed into the frequency bands that represent the cyclical motion of the water surface. The JONSWAP frequency spectra were created using the wave parameters: significant wave height, peak period, and mean wave direction and the two terms alpha and gamma which govern the spectral shape. For this study, The JONSWAP frequency spectra was computed using standard empirical values of $\gamma = 3.3$, and $\sigma_a = 0.07$ and $\sigma_b = 0.09$ (Hasselmann et al. 1973). The JONSWAP method creates parametric frequency spectra, where energy is placed around the peak frequency and less energy is placed into the higher frequencies. Thus, the FFT generated spectra have more variability than the parametric frequency spectra, but the peak frequency and integrated energy density are the same because the FFT output of these parameters is specified as the JONSWAP input.

The directional spreading functions LH, MLM, and MEM use the co and quad directional coefficients derived from the FFT of the buoy's pitch and roll. The LH spreading function spreads energy in broad arcs about the mean wave direction. The

result is wave spectra resembling a wind sea where energy is more diffused over directions. The MLM spreading function is more narrowly arced than LH, with each frequency band skewed towards the mean wave direction. The wave spectra for MLM resembles something between wind sea and swell. The MEM spreading function spreads energy very narrowly over few directions and resembles wave spectra more like swell where energy is propagating from one main direction. The FFT coefficient spreading functions spread each frequency independently based on the coefficient generated for each frequency band.

The Cos^2 and Cos^{2s} spreading functions spread the energy parametrically around the mean wave direction. The Cos^2 spreading function bands the energy ± 90 degrees about the mean wave direction in a cosine squared shape. The Cos^{2s} spreading function also spreads energy in a cosine squared shape, but uses an "s" parameter to describe the shape of the peak. The "s" parameter was calculated using Cartwright's method (1963) whereby "s" is related to the first order FFT coefficients. This method was chosen due to the availability of the measured data from the NDBC buoy. Since the "s" values are calculated based on the FFT coefficients, the value changes for each frequency band and each time interval. A single spectrum's "s" parameter can range from approximately 0.06 to 5. Other methods for calculating "s" include Mitsuyasu et al. (1975) which show a correspondence between the maximum spreading parameter and the peak frequency, Goda's (1985) method which assigns constant values dependent on the wave climate, and Wang's (1992) method which show 's' has a relationship with wavelength and peak frequency. The cosine parametric spreading functions, unlike the FFT coefficient

spreading functions, apply the same spread to each frequency band because there is no individual frequency information retained in their creation.

The model spectral outputs were evaluated without tides or winds, with the addition of tides, and with the addition of winds to determine the effects these conditions had on the evolution of the spectra. The average diurnal tidal range for the Mississippi Sound is 0.45 to 0.51 meters (Eleuterius et al. 1979). To test the tidal influence, the water elevation was adjusted to reflect the average diurnal range (±0.5 m). STWAVE was also run with winds. When winds were included, the wind data was retrieved from the same NDBC buoy as the wave data for the time period. The most prevailing wind direction for the time period was approximately 160 degrees or headed toward the northwest. The maximum wind speed was 7.7 m/s from 163 degrees and the minimum wind speed was 1.5 m/s from 169 degrees. Other model input conditions included a constant JONSWAP bottom friction coefficient of 0.04, as suggested by van Vledder et al. (2011) for sandy beds. The single low friction factor is applicable in the area due to the assumption that the low variation in bottom friction values is not great enough to affect wave transformation. No currents were applied, as the mild environment makes the occurrence of strong currents capable of affecting wave propagation unlikely.

3.1.2 Grid Boundary Effect on Spectra

At the buoy location, the energy is measured over the full 360-degrees plane (Figure 3.2). This generates spectra directionally spread from 0 to 360 degrees. However, within the model grid only wave energy propagating in the direction into the grid was used within the model. The spectra were thus truncated ± 85-degrees about the grid azimuth (Figure 3.3). Therefore, due to the varying shapes of the different directional

wave spectra and the varying mean wave directions over time, the amount of energy propagating into the grid can be different between each simulation directional distribution type due to truncation.

The Cos^2 function was the most affected by truncation, due to the wide, ± 90 degree banding about the mean wave direction. To quantify the amount of energy lost due to truncation of the parametric spreading function, a test was conducted. For this test, a 3-year, 30-month record from 2015 to 2017, from the NDBC buoy 42040 (the same buoy used in this study) was analyzed to determine percent energy truncated based on the grid orientation using Cos^2. The analysis determined that over the 3-year record, on average 40 percent of the spectral energy was lost. When the mean wave direction was propagating in a direction outside of the grid domain, the energy losses increased. For example, from the 3-year record, May, 1, 2015 at 3:50 am, 65 percent of the spectral energy was truncated because the mean wave direction (270 degrees) was propagating outside of the grid, so that more than half of the spectral energy was lost. Losses on the order of 90 percent or greater occurred when the mean wave direction was propagating near 180 degrees away from the grid's azimuth. This extreme truncation occurred for 3 percent of the record.

During the 3-day time period for this study, there were two occurrences, September 17, 2016 10:40 and September 18, 2016 00:40, when the Cos^2 parametric function caused an extreme truncation of energy in the spectra. The mean wave directions associated with these time periods are 289 degrees and 288 degrees which is almost completely 180 degrees away from the grid's azimuth. Thus, the result of using the Cos^2

spreading function under these conditions resulted in larger losses of spectral energy and ultimately impacted the reported wave parameters within the nearshore model.

Figure 3.2 shows the five spectra as generated at the offshore buoy with energy placed in the full 360 degrees orientation. Figure 3.3 shows the five spectra as input into the model grid. Inside the model only those waves moving ± 85 degrees about the grid's azimuth (116 degrees) are included. From this truncation, shown in Figure 3.3, the effect of the narrow direction banding with the Cos^2 spreading function results in lower amounts of energy being input into the model compared to the other spreading functions.

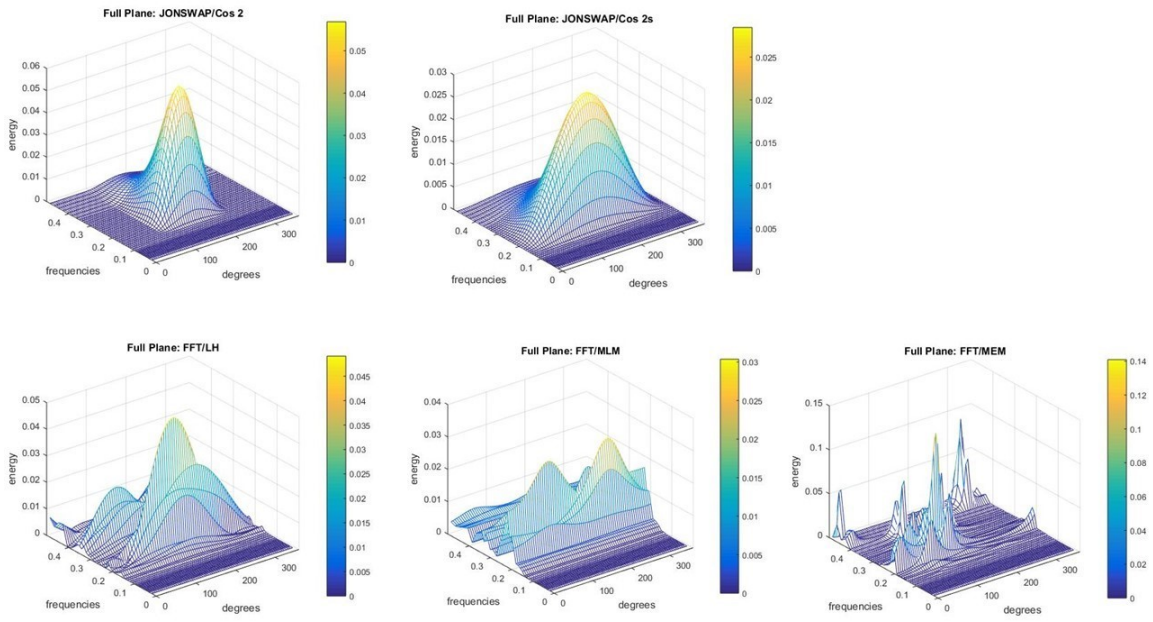

Figure 3.2 360 degree directional wave spectra

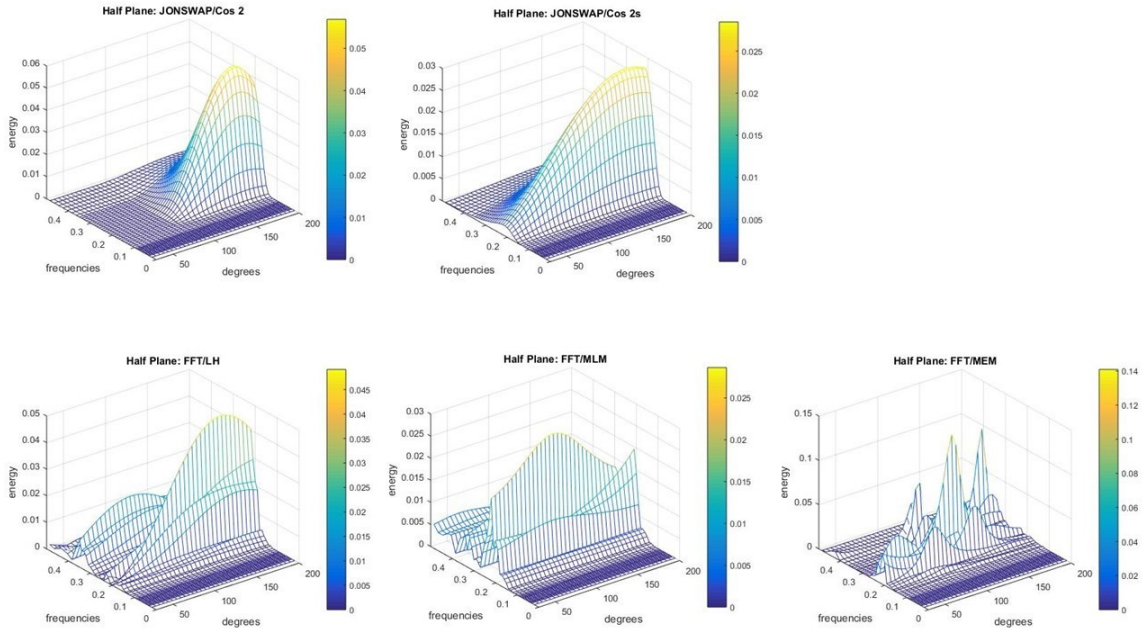

Figure 3.3 180 degree directional wave spectra.

Table 3.1 gives the deepwater wavelength and maximum water depth at which waves of that length interact with the bottom (depth = 0.5 x wavelength) for the range of wave frequencies used in these analyses. The most common peak frequency (period) for the time period was approximately 0.22 Hz (4.5 sec), indicating that this wave would interact with the bottom at a depth of 16 meters or less, which in the bathymetry grid (Figure 2.1) correlates with the area landward of the barrier islands. The energy for all spectra was generally placed in the frequencies 0.17 to 0.40 Hz, meaning wave-bottom interactions occurred in water depths of 3.30 to 27 m. The frequencies less than 0.17 Hz feel the bottom in depths deeper than the model grid bathymetry, however, there is little to no energy in these frequencies for this time period.

Table 3.2 Relationship between Wave Frequency, Deep Water Wave Length and Minimum Depth for Wave Interaction with the Bottom

Frequency (Hz)	Wavelength (m)	Depth (m):	Frequency (Hz)	Wavelength (m)	Depth (m):
0.11	129.0	64.5	0.27	21.4	10.7
0.12	108.4	54.2	0.27	21.4	10.7
0.13	92.4	46.2	0.28	19.9	10.0
0.14	79.7	39.8	0.29	18.6	9.3
0.15	69.4	34.7	0.30	17.3	8.7
0.16	61.0	30.5	0.31	16.2	8.1
0.17	54.0	27.0	0.32	15.2	7.6
0.18	48.2	24.1	0.33	14.3	7.2
0.19	43.2	21.6	0.34	13.5	6.8
0.20	39.0	19.5	0.35	12.7	6.4
0.21	35.4	17.7	0.37	11.7	5.9
0.22	32.3	16.1	0.39	10.5	5.3
0.23	29.5	14.8	0.41	9.5	4.8
0.24	27.1	13.6	0.43	8.6	4.3
0.25	25.0	12.5	0.45	7.9	3.9
0.26	23.1	11.5			

3.1.3 Method for Analysis

STWAVE transforms wave energy and direction as a function of wave-bottom interactions. In general, waves will interact and align with the bottom contours through refraction and wave heights will increase and then decrease due to shoaling and breaking in shallow depths. The inclusion of islands in the domain also reduces wave height in their lee through sheltering. These transformation processes are dependent on wave frequency and direction. Therefore, the differences in the input wave spectra will result in differences in the transformation processes. Wave source terms of wind-driven growth and dissipation due to bottom friction are also dependent on wave direction and frequency. The model spectral outputs reflect both wave transformation and source terms

across the grid and differences due to the input directional wave spectral computation method at the boundary. The wave transformation of each directional wave spectrum will differ spectral component by spectral component because they are dependent on the frequency and direction of the wave component. To quantify the differences due to the five directional wave spectra, a demeaned root-mean-square difference (RMSE), a bias, and a Pearson correlation coefficient were calculated for all. A percent difference was also included for wave heights and peak period parameters.

The root-mean-square difference is a measure of how much the values in each experiment differ from one another, with 0.0 indicating no difference. The RMSE was calculated as:

$$RMSE = \sqrt{\frac{1}{N-1}\sum(y_i - x_i - b)^2} \tag{3.1}$$

Where, RMSE is the root-mean-square difference, N is the total number of measurements, y_i represents the experimental run being compared against, x_i represents the experimental run of interest, and b is the bias.

The bias is a statistical representation of when one experimental run gives consistently greater or lesser values than the other experimental runs. If the bias value is positive then, the experimental run of interest is larger than the baseline value. If the bias value is negative, then the experimental run is smaller than the baseline values. This was determined by:

$$b = \frac{1}{N}\sum(y_i - x_i) \tag{3.2}$$

Percent difference is used when the datasets being compared have differing means, in order to normalize the differences to compare the RMSE values. The RMSE is divided by the mean giving a percent difference which can be used for comparisons.

The sample Pearson correlation coefficient, *corr*, is a statistical representation of linear correlation between two model runs of interest. A perfect linear relationship has a value of 1.0 with positive values indicating an increasing linear relationship and negative values indicating a decreasing linear relationship. A value of 0.0 indicates no linear relationship. The sample Pearson correlation coefficient was defined as:

$$corr = \frac{\sum(X_i - \bar{X})(Y_i - \bar{Y})}{\sqrt{\sum(X_i - \bar{X})^2}\sqrt{\sum(Y_i - \bar{Y})^2}} \tag{3.3}$$

Where, $\overline{X}$ is the mean of the experimental run of interest, and $\overline{Y}$ is the mean of the experimental run being compared against.

CHAPTER IV

RESULTS

The purpose of this section is to quantify the differences in each spectral method output from STWAVE under the conditions with and without tides and with and without winds.

4.1 Tide

A test was run to determine the effect of tides by adjusting the water elevation ±0.5 m to account for the diurnal tide in the area, as well as a run with no water elevation adjustment. The test included the five directional wave spectra, and the 0.04 JONSWAP constant bottom friction value. The results when compared to no water level adjustments showed that the tide did change some values in the wave parameters, but these changes occurred for all spectra and therefore the water elevation adjustment did not cause any changes to the results in one spectral method versus another. The Pearson correlation values equaled 1 between with tide and without, showing that the trend in outputs between all the spectra did not change with the water elevation adjustment. The tides did cause differences in values for the integral wave parameters, but these differences were constant for all spectra. The water elevation adjustment caused an increase in wave height of 1 cm at the boundary and at the barrier islands, but no changes in wave height in the nearshore. For peak period, differences of about 0.2 seconds occurred at the boundary and barrier islands, with no differences at the nearshore. The mean wave direction had

no changes due to the addition of the tide. The increase in water elevation did affect the values of the three wave parameters; however, these differences occurred for all spectra and therefore did not cause any more or less differences between the spectral methods.

4.2 Winds

A test was performed with and without winds to investigate the effects of the winds on the performance of each spectral method. The results showed that the winds had a significant impact on the model results for each spectral method. With winds, the overall wave energy was higher and differences in the spectra's output wave parameters were masked at the barrier islands and nearshore. The differences were masked because the wave energy was low enough that the winds began to dominate the direction and magnitude of the waves. Without winds, the results showed that the overall energy was lower and the differences in the spectra were preserved from the offshore to the nearshore.

4.2.1 Wave Height

For all spectral inputs, both with and without winds, the output wave height decreased towards shore. However, with winds, the wave heights were greater than without winds. The RMSE statistic quantitated how different the outputs of each spectral method were from one another. With winds, the RMSE values ranged from 0.00 m to 0.05 m and without winds, the values ranged 0.01 m to 0.09 m (Table 4.1-4.2). These values indicate that differences between wave heights were less with winds, than without winds.

However, because the mean significant wave heights are different with and without winds, percent difference, a statistic which normalizes these differences, was used to compare each spectrum with and without applied winds. The percent difference without winds increased slightly towards shore for the JONSWAP (J) generated spectra compared to the FFT (F) generated spectra. Indicating that differences between the JONSWAP generated spectra and FFT generated spectra increased towards shore without winds (24%-48% at boundary, 37-64% at nearshore). With winds the difference decreased towards shore between JONSWAP and FFT generated spectra (51-96% at boundary, 38-63% at nearshore). The greatest percent difference (102%) occurred without winds, between J Cos^2 and F MEM at the nearshore (Table 4.2). With winds, the greatest percent difference (105%) occurred between F MEM and J Cos^{2s} at the barrier Islands. J Cos^2 / J Cos^{2s} and F MEM are very differently shaped spectra. The MEM creates very narrow peaks of energy applied differently per each frequency bands, while the Cos^2 and Cos^{2s} functions create single peaks about the mean wave direction in parametric spreads of energy and applied to all frequency bands.

The bias with and without winds showed that the JONSWAP generated spectra tended to produce lower wave heights when compared to the FFT generated spectra, as the bias values were negative (Table 4.1 and Table 4.2). In general, the JOSNWAP generated frequency spectra were most similar to themselves, with a bias range between 0.0 to 0.1 m without winds and -0.01 to 0.23m with winds. The similarity and low bias between J Cos^2 and J Cos^{2s} is indicative of the similar energy placement per frequency band between the two methods. Between the FFT generated frequency spectra, F MEM often output lower wave heights than F LH or F MLM, except in the nearshore were the

bias was 0.0 m for both with and without winds. F MEM placed energy more narrowly and therefore, changes to that frequency band resulted in lower energy levels for the F MEM method that were not seen in F LH and FMLM which placed energy more broadly. The bias for all spectra methods increased (0.01 m to 0.23 m at the boundary 0.0 m to 0.06 m at the barrier islands, and 0.0 m to 0.01 m at the nearshore) with the application of winds and the increased energy within the system.

The Pearson correlation values indicate the linear relationship between the spectral method outputs, or how well the spectral methods followed the same trend. The closer the correlation value is to 1, the more linear or equivalent, the relationship. The Pearson correlation values with and without winds were greatest (closest to 1) between similarly generated frequency spectra at the boundary (i.e., $JCos^2$ and $JCos^{2s}$ or FFT methods). With winds, the Pearson correlation values between JONSWAP generated frequency spectra and FFT generated frequency spectra increased towards shore (Table 4.2) from 0.12 - 0.40 at the boundary to 0.75 to 0.91 at the nearshore. The increase means that with the addition of winds the relationship is more linear for differently generated spectra as the winds begin to dominate in the barrier island and nearshore regions. Without winds, there is no improvement in Pearson correlation values between differently generated boundary spectra and in some cases, like between F LH and J Cos2, the Pearson correlation worsened from 0.06 at the boundary to -0.03 in the nearshore. A lack of improvement in correlation values indicates that without wind, the spectra did not converge in the nearshore, like what occurred with wind (Table 4.1).

It is important to note that the boundary output point under the “with winds” condition would have been more affected by the winds if the model domain had extended

to the buoy 85km away. However, for the purposes of this study the boundary point within the model grid was used as a marker to determine whether the spectra maintain their differences immediately within the model domain, and as shown by the statistics and the model outputs, even with the inclusion of winds, the spectral differences are maintained.

Table 4.1 Wave Height (m) (Hmo) without winds

	Mean	RMSE	Bias	% error	Corr	RMSE	Bias	% error	Corr	RMSE	Bias	% error	Corr	RMSE	Bias	% error	Corr	RMSE	Bias	% error	Corr
Boundary		J Cos2				J Cos2s				F LH				F MLM				F MEM			
J Cos2	0.08					0.02	0.01	28%	0.97	0.05	0.02	58%	0.06	0.04	0.01	56%	0.14	0.05	0.03	58%	0.10
J Cos2S	0.08	0.02	-0.01	26%	0.97					0.03	0.01	31%	0.19	0.02	0.01	26%	0.36	0.02	0.02	30%	0.25
F LH	0.10	0.05	-0.02	48%	0.06	0.03	-0.01	27%	0.19					0.02	0.00	17%	0.47	0.01	0.01	7%	0.93
F MLM	0.09	0.04	-0.01	48%	0.14	0.02	-0.01	24%	0.36	0.02	0.00	17%	0.47					0.01	0.01	15%	0.62
F MEM	0.10	0.05	-0.03	43%	0.10	0.02	-0.02	24%	0.25	0.01	-0.01	6%	0.93	0.01	-0.01	13%	0.62				
Barrier Island		J Cos2				J Cos2s				F LH				F MLM				F MEM			
J Cos2	0.02					0.01	0.00	49%	0.88	0.02	0.01	97%	-0.07	0.02	0.01	90%	0.03	0.02	0.02	97%	-0.04
J Cos2S	0.03	0.01	0.00	42%	0.88					0.01	0.01	50%	0.07	0.01	0.00	42%	0.25	0.01	0.01	50%	0.11
F LH	0.03	0.02	-0.01	65%	-0.07	0.01	-0.01	39%	0.07					0.01	0.00	22%	0.42	0.01	0.00	17%	0.78
F MLM	0.03	0.02	-0.01	66%	0.03	0.01	0.00	36%	0.25	0.01	0.00	24%	0.42					0.01	0.01	25%	0.46
F MEM	0.04	0.02	-0.02	57%	-0.04	0.01	-0.01	35%	0.11	0.01	0.00	14%	0.78	0.01	-0.01	20%	0.46				
Nearshore		J Cos2				J Cos2s				F LH				F MLM				F MEM			
J Cos2	0.01					0.00	0.00	52%	0.87	0.01	0.00	99%	-0.03	0.01	0.00	93%	0.09	0.01	0.00	102%	-0.02
J Cos2S	0.01	0.00	0.00	43%	0.87					0.00	0.00	50%	0.16	0.00	0.00	44%	0.30	0.00	0.00	55%	0.12
F LH	0.01	0.01	0.00	64%	-0.03	0.00	0.00	39%	0.16					0.00	0.00	17%	0.69	0.00	0.00	18%	0.78
F MLM	0.01	0.01	0.00	64%	0.09	0.00	0.00	37%	0.30	0.00	0.00	18%	0.69					0.00	0.00	25%	0.54
F MEM	0.01	0.01	0.00	59%	-0.02	0.00	0.00	38%	0.12	0.00	0.00	16%	0.78	0.00	0.00	21%	0.54				

Mean, RMSE, Bias, percent difference, and the Pearson correlation coefficient between wave height outputs without winds

Table 4.2 Wave Height (m) (Hmo) with winds

	Mean	RMSE	Bias	% error	Corr	RMSE	Bias	% error	Corr	RMSE	Bias	% error	Corr	RMSE	Bias	% error	Corr	RMSE	Bias	% error	Corr
Boundary		J Cos2				J Cos2s				F LH				F MLM				F MEM			
J Cos2	0.09					0.05	0.23	53%	0.92	0.07	0.24	85%	0.12	0.06	0.23	69%	0.26	0.07	0.27	82%	0.16
J Cos2S	0.09	0.05	-0.23	51%	0.92					0.10	0.01	107%	0.18	0.08	0.00	90%	0.40	0.09	0.04	101%	0.27
F LH	0.10	0.07	-0.24	73%	0.12	0.10	-0.01	96%	0.18					0.06	-0.01	59%	0.44	0.02	0.03	20%	0.94
F MLM	0.10	0.06	-0.23	61%	0.26	0.08	0.00	83%	0.40	0.06	0.01	60%	0.44					0.05	0.04	49%	0.62
F MEM	0.11	0.07	-0.27	65%	0.16	0.09	-0.04	84%	0.27	0.02	-0.03	19%	0.94	0.05	-0.04	44%	0.62				
Barrier Island		J Cos2				J Cos2s				F LH				F MLM				F MEM			
J Cos2	0.06					0.04	0.06	77%	0.79	0.05	0.07	92%	0.69	0.03	0.06	56%	0.88	0.05	0.09	94%	0.68
J Cos2s	0.06	0.04	-0.06	77%	0.79					0.06	0.01	104%	0.62	0.04	0.00	69%	0.82	0.06	0.03	105%	0.61
F LH	0.06	0.05	-0.07	82%	0.69	0.06	-0.01	92%	0.62					0.04	-0.01	58%	0.84	0.01	0.02	22%	0.98
F MLM	0.06	0.03	-0.06	54%	0.88	0.04	0.00	66%	0.82	0.04	0.01	62%	0.84					0.04	0.03	65%	0.82
F MEM	0.07	0.05	-0.09	80%	0.68	0.06	-0.03	90%	0.61	0.01	-0.02	21%	0.98	0.04	-0.03	57%	0.82				
Nearshore		J Cos2				J Cos2s				F LH				F MLM				F MEM			
J Cos2	0.03					0.01	0.01	51%	0.84	0.02	0.01	62%	0.77	0.01	0.01	45%	0.87	0.02	0.02	63%	0.75
J Cos2S	0.03	0.01	-0.01	52%	0.84					0.02	0.00	60%	0.79	0.01	0.00	39%	0.91	0.02	0.00	62%	0.77
F LH	0.03	0.02	-0.01	62%	0.77	0.02	0.00	58%	0.79					0.01	0.00	40%	0.89	0.00	0.00	16%	0.98
F MLM	0.03	0.01	-0.01	45%	0.87	0.01	0.00	38%	0.91	0.01	0.00	41%	0.89					0.01	0.00	43%	0.87
F MEM	0.03	0.02	-0.02	63%	0.75	0.02	0.00	60%	0.77	0.00	0.00	16%	0.98	0.01	0.00	43%	0.87				

Mean, RMSE, Bias, percent difference and the Pearson correlation coefficient between wave height outputs with winds

The model outputs through time visually display the performance of each spectral method with and without winds (figure 4.1 to figure 4.3). At the boundary, the wave heights without winds were lower than with winds (figure 4.1). However, the output trends or differences in reported wave heights between the spectral methods were maintained regardless of wind input. With and without winds on the boundary, J Cos^2 and J Cos^{2s} had the most variance in outputs. The greater amount of variance in the JONSWAP generated spectra were likely do to the deviance of the mean wave direction and the resulting truncation of the spectra.

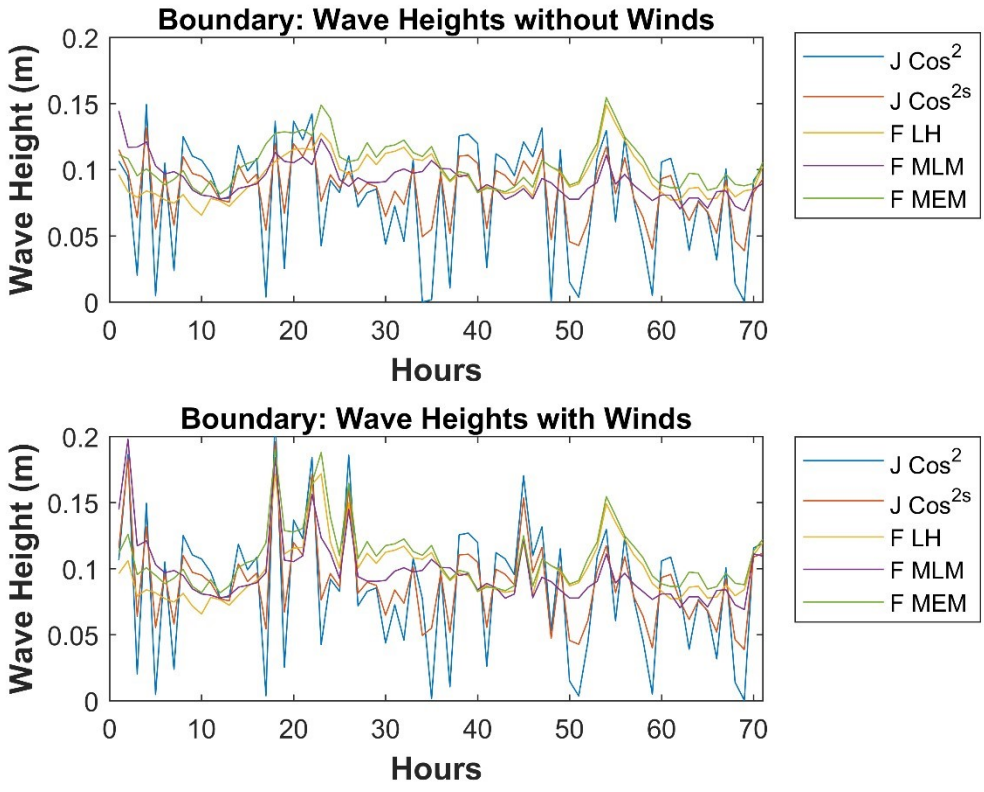

Figure 4.1 Time series of significant wave heights at the boundary point with and without winds for the five spectral methods

The wave heights without winds at the barrier island were lower than with winds and show greater differences between the spectral methods (figure 4.2). With winds, the outputs look more uniform and the differences were not as pronounced

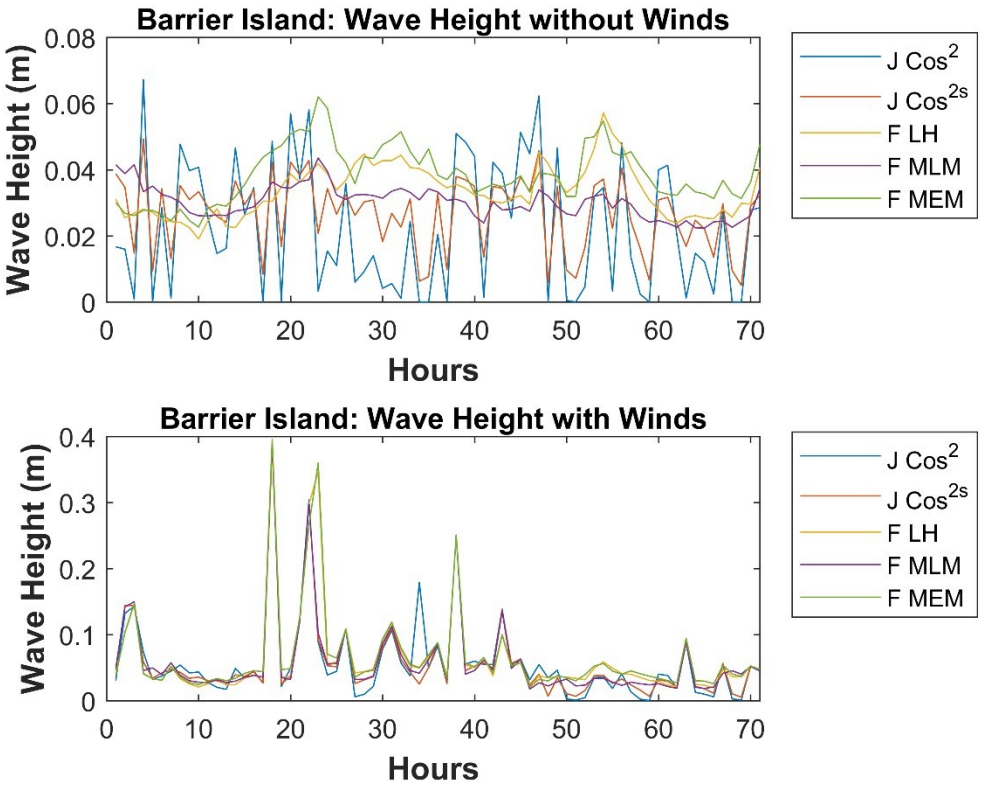

Figure 4.2 Time series of the significant wave height at the barrier island point with and without winds for the five spectral methods

In the nearshore, the wave heights without winds were lower, and still reflected the differences between each spectrum, as seen on the boundary (figure 4.3). However, with the application of winds, the wave heights were greater and the outputs were more uniform across spectral methods. Therefore, the differences in spectral method seen at the

boundary were not observed with winds because the winds dominate the wave energy at this location as clearly shown in Figure 4.3b.

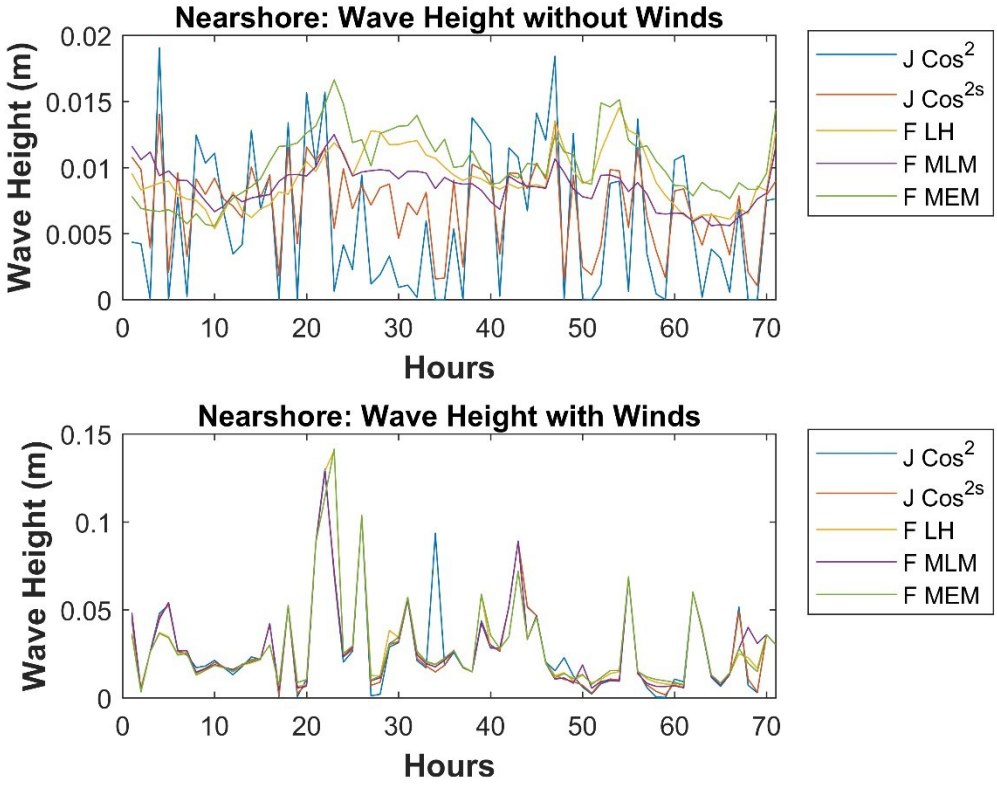

Figure 4.3 Time series of significant wave heights at the nearshore point with and without winds

4.2.2 Peak Period

The peak period values decreased towards shore, with and without winds, with the greatest decreases occurring in the nearshore (Table 4.3 and Table 4.4). The decrease in peak period nearshore was because the higher frequencies persisted further into the model grid. Higher frequencies do not undergo wave bottom interactions and transformations like the lower frequencies, because they do not penetrate as deeply and therefore will not

transform until in shallower depth waters. The RMSE and percent difference values indicate how differently one spectral method is from another. The RMSE values ranged from 0.29 sec to 1.48 sec without winds and from 0.30 sec to 1.17 sec with winds (Tables 4.3 and Table 4.4).The RMSE and percent difference values with and without winds increased towards shore, meaning the differences between the spectral outputs were more pronounced as they transformed from the offshore to the nearshore.

The bias shows the trend of a spectral method to produce longer or shorter peak periods compared to the other spectral methods, with positive values indicating longer periods and negative values indicating shorter periods. The bias, without winds, showed that J Cos^2 and F MLM tend to output shorter peak periods than the other spectra (Table 4.3). With winds, the bias showed that J Cos^2, J Cos^{2s}, and F MLM output shorter peak periods (Table 4.4). The ability to produce shorter peak periods indicates that these spectra have more energy placed in higher frequencies than the other spectra.

The Pearson correlation values indicate the linear relationship between the spectral outputs. The closer the correlation value is to 1, the more linear the relationship. The Pearson correlation values with and without winds were greatest between similarly generated frequency spectra. With winds, the correlation values were higher at all locations than without winds, which indicate that the wind dominates and the boundary spectra are less important to the local wave conditions when winds are present. The correlation values, with winds, increased from the boundary to the nearshore (0.28 to 0.78 at the boundary, 0.61 to 0.91 at the nearshore), but without winds, the correlation values decreased from 0.40 to 0.70 at the boundary to 0.01 to 0.61 in the nearshore.

Table 4.3 Peak Period (sec) (Tp) without winds

	Mean	RMSE	Bias	% error	Corr	RMSE	Bias	% error	Corr	RMSE	Bias	% error	Corr	RMSE	Bias	% error	Corr	RMSE	Bias	% error	Corr
Boundary		J Cos2				J Cos2s				F LH				F MLM				F MEM			
J Cos2	4.63					0.40	0.07	9%	0.70	0.57	0.32	12%	0.40	0.51	0.04	11%	0.52	0.59	0.34	13%	0.33
J Cos2S	4.70	0.40	-0.07	9%	0.70					0.46	0.25	10%	0.42	0.31	-0.03	7%	0.76	0.49	0.27	10%	0.29
F LH	4.95	0.57	-0.32	11%	0.40	0.46	-0.25	9%	0.42					0.52	-0.28	11%	0.37	0.29	0.03	6%	0.79
F MLM	4.67	0.51	-0.04	11%	0.52	0.31	0.03	7%	0.76	0.52	0.28	11%	0.37					0.56	0.31	12%	0.26
F MEM	4.98	0.59	-0.34	12%	0.33	0.49	-0.27	10%	0.29	0.29	-0.03	6%	0.79	0.56	-0.31	11%	0.26				
Barrier Island		J Cos2				J Cos2s				F LH				F MLM				F MEM			
J Cos2	4.56					0.61	0.15	13%	0.51	0.88	0.09	19%	0.15	0.75	-0.17	17%	0.21	0.81	0.14	18%	0.25
J Cos2S	4.70	0.61	-0.15	13%	0.51					0.63	-0.05	13%	0.31	0.44	-0.32	9%	0.43	0.57	-0.01	12%	0.42
F LH	4.65	0.88	-0.09	19%	0.15	0.63	0.05	14%	0.31					0.59	-0.26	13%	0.45	0.30	0.04	6%	0.89
F MLM	4.39	0.75	0.17	17%	0.21	0.44	0.32	10%	0.43	0.59	0.26	13%	0.45					0.62	0.31	14%	0.34
F MEM	4.69	0.81	-0.14	17%	0.25	0.57	0.01	12%	0.42	0.30	-0.04	6%	0.89	0.62	-0.31	13%	0.34				
Nearshore		J Cos2				J Cos2s				F LH				F MLM				F MEM			
J Cos2	4.30					0.96	0.40	22%	0.33	1.47	-0.56	34%	-0.01	1.32	-0.45	31%	0.02	1.48	-0.44	34%	-0.05
J Cos2S	4.70	0.96	-0.40	20%	0.33					1.01	-0.96	21%	0.26	0.85	-0.86	18%	0.27	0.99	-0.84	21%	0.27
F LH	3.74	1.47	0.56	39%	-0.01	1.01	0.96	27%	0.26					1.03	0.10	27%	0.43	1.13	0.12	30%	0.41
F MLM	3.85	1.32	0.45	34%	0.02	0.85	0.86	22%	0.27	1.03	-0.10	27%	0.43					0.85	0.02	22%	0.61
F MEM	3.87	1.48	0.44	38%	-0.05	0.99	0.84	26%	0.27	1.13	-0.12	29%	0.41	0.85	-0.02	22%	0.61				

Mean, RMSE, Bias, percent difference and the Pearson correlation coefficient between peak period outputs without winds

Table 4.4 Peak Period (sec) (Tp) with winds

	Peak Period Tp--with winds (sec)																			
	Mean	RMSE	Bias	% error	Corr	RMSE	Bias	% error	Corr	RMSE	Bias	% error	Corr	RMSE	Bias	% error	Corr	RMSE	Bias	% error	Corr
Boundary		J Cos2				J Cos2s				F LH				F MLM				F MEM			
J Cos2	4.66					0.38	0.07	8%	0.72	0.56	0.32	12%	0.40	0.50	0.03	11%	0.54	0.58	0.35	13%	0.33
J Cos2S	4.73	0.38	-0.07	8%	0.72					0.46	0.25	10%	0.41	0.31	-0.04	7%	0.76	0.49	0.29	10%	0.28
F LH	4.98	0.56	-0.33	11%	0.40	0.46	-0.25	9%	0.41					0.52	-0.29	11%	0.37	0.30	0.03	6%	0.78
F MLM	4.69	0.50	-0.03	11%	0.54	0.31	0.04	7%	0.76	0.52	0.29	11%	0.37					0.56	0.32	12%	0.27
F MEM	5.01	0.58	-0.35	12%	0.33	0.49	-0.29	10%	0.28	0.30	-0.03	6%	0.78	0.56	-0.32	11%	0.27				
Barrier Island		J Cos2				J Cos2s				F LH				F MLM				F MEM			
J Cos2	4.37					0.79	0.24	18%	0.61	1.05	0.30	24%	0.32	0.98	-0.01	23%	0.36	1.06	0.30	24%	0.26
J Cos2S	4.61	0.79	-0.24	17%	0.61					0.73	0.06	16%	0.52	0.69	-0.26	15%	0.52	0.76	0.06	16%	0.43
F LH	4.67	1.05	-0.30	22%	0.32	0.73	-0.06	16%	0.52					0.76	-0.31	16%	0.47	0.40	0.00	9%	0.85
F MLM	4.36	0.98	0.01	23%	0.36	0.69	0.26	16%	0.52	0.76	0.31	17%	0.47					0.72	0.31	17%	0.47
F MEM	4.67	1.06	-0.30	23%	0.26	0.76	-0.06	16%	0.43	0.40	0.00	9%	0.85	0.72	-0.31	16%	0.47				
Nearshore		J Cos2				J Cos2s				F LH				F MLM				F MEM			
J Cos2	3.44					0.58	0.02	17%	0.91	1.09	-0.25	32%	0.67	0.81	-0.23	24%	0.82	1.17	-0.32	34%	0.61
J Cos2S	3.46	0.58	-0.02	17%	0.91					0.89	-0.27	26%	0.78	0.72	-0.25	21%	0.86	1.05	-0.34	30%	0.69
F LH	3.19	1.09	0.25	34%	0.67	0.89	0.27	28%	0.78					0.78	0.01	25%	0.82	0.70	-0.07	22%	0.85
F MLM	3.20	0.81	0.23	25%	0.82	0.72	0.25	23%	0.86	0.78	-0.01	24%	0.82					0.91	-0.09	28%	0.75
F MEM	3.12	1.17	0.32	38%	0.61	1.05	0.34	34%	0.69	0.70	0.07	23%	0.85	0.91	0.09	29%	0.75				

Mean, RMSE, Bias, percent difference and the Pearson correlation coefficient between peak period outputs with winds

The differences between peak periods with and without winds are visible when graphed through time (figure 4.4-figure 4.6). At the boundary, the peak periods were approximately 4-5 seconds for all spectra with and without winds. J Cos^2 had two significant reductions in peak periods (figure 4.4). The Cos^2 spreading function caused truncation of the spectra to the extent that it created an almost zero spectrum on September 17, 2016 10:40 am and September 18, 2016 00:40 am. This phenomenon occurred when the mean wave direction was near 180 degrees away from the grid azimuth at an angle of 289 degrees and 288 degrees. The truncation did not occur for the other methods even though they too had the same mean period because of the banding ± 90 degrees about the mean wave direction and the truncation of energy not heading into the model grid.

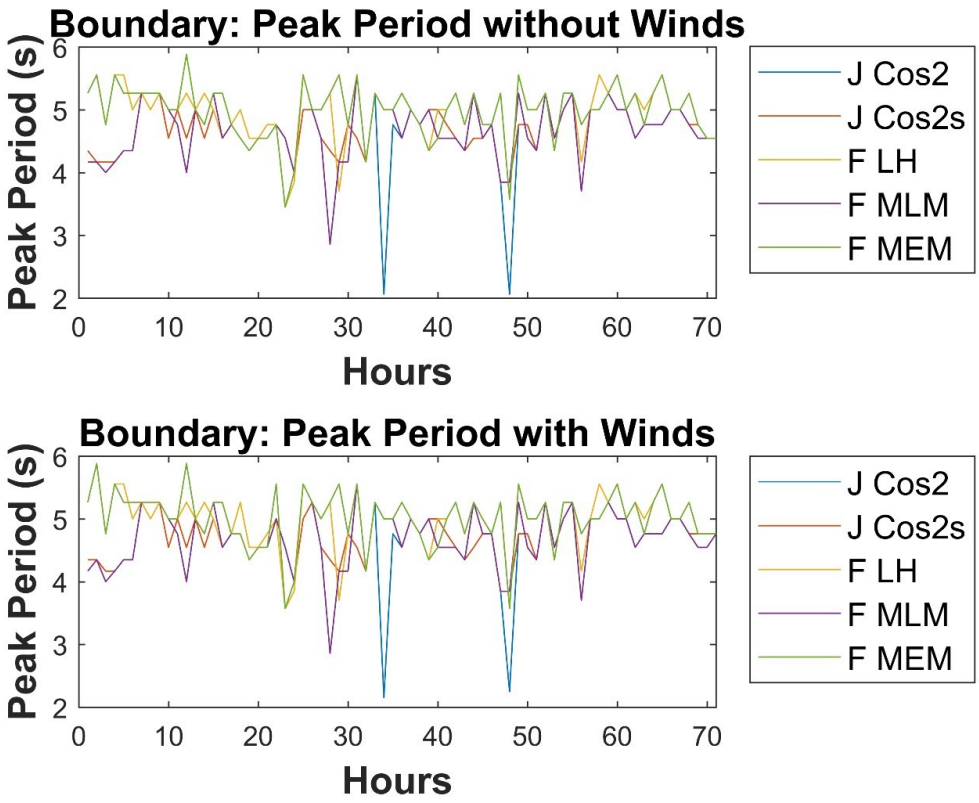

Figure 4.4 Time series of peak period at the boundary point with and without winds

At the barrier island, more differences between with and without winds were evident in the time series (figure 4.5). The peak periods without winds ranged about 4-5 seconds, with J Cos^2 showing deviations due to energy losses in the spectra. These spectral energy losses occur when the mean wave direction is headed outside of the model domain. With winds, the peak periods ranged was 3-5 seconds and showed more variance throughout the time series.

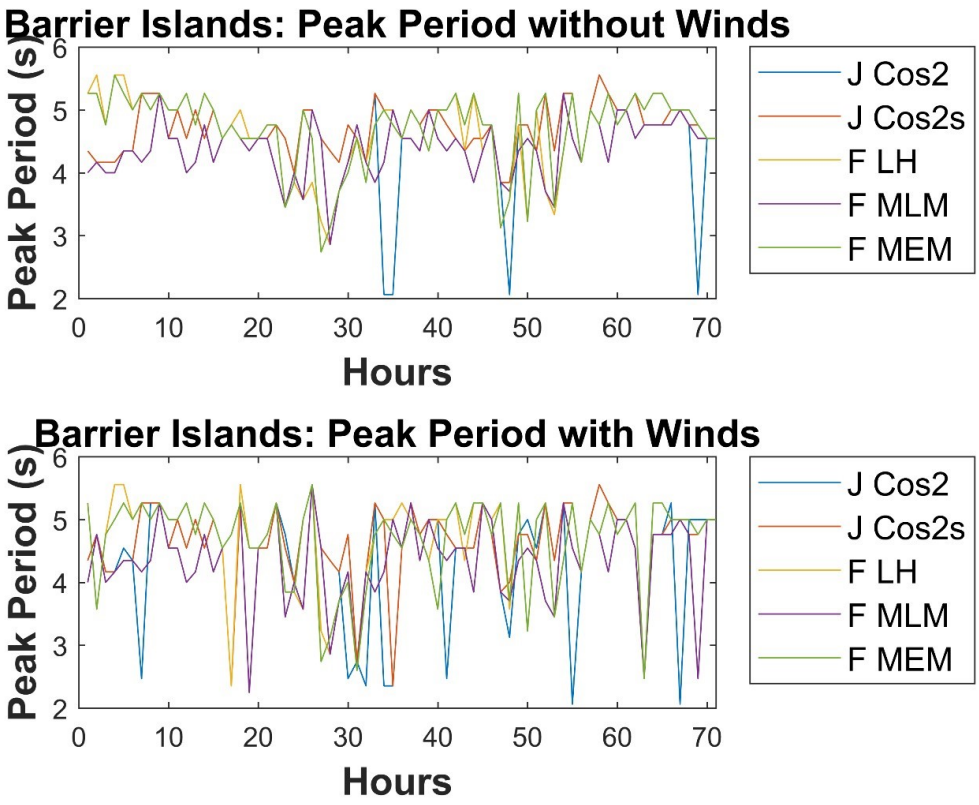

Figure 4.5 Time series of the peak periods at the barrier island point with and without winds

In the nearshore, the wind's influence on peak period was observed for all spectra (figure 4.6). The peak period without winds ranged from 2 to 5 seconds with no clear trend between the spectral methods. The peak period with winds for all spectra also ranged from 2 to 5 seconds, except a clear similarity in values was observed between the spectral methods.

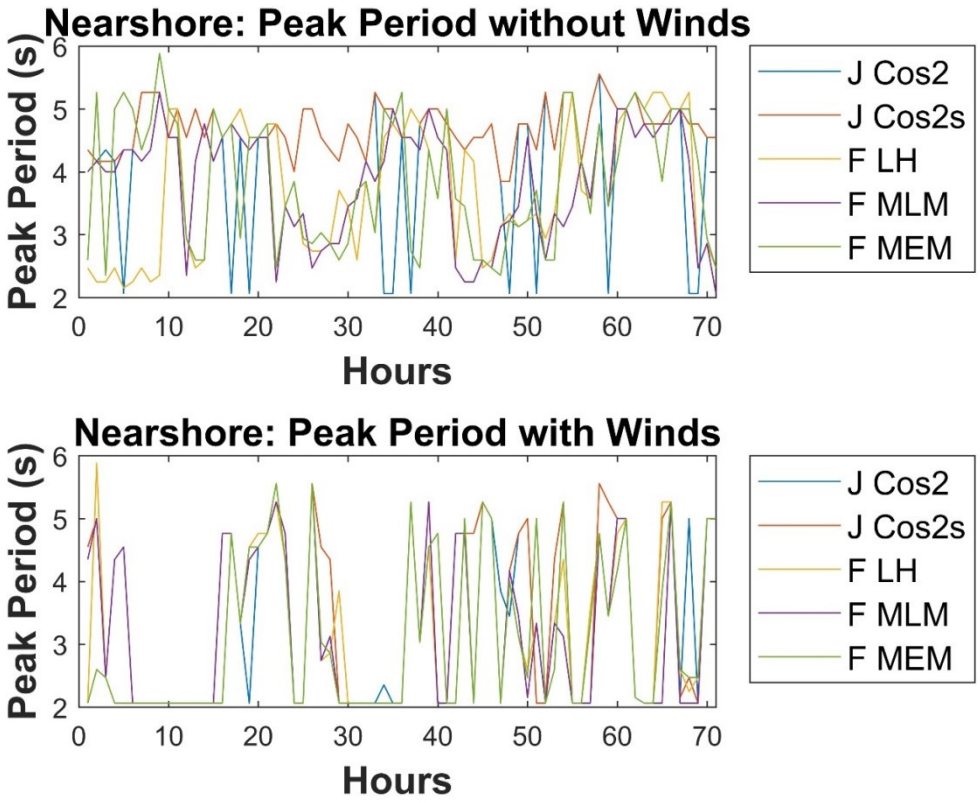

Figure 4.6 Time series of peak period at the nearshore point with and without winds

4.2.3 Mean Wave Direction

During the simulation period the mean wave direction rotated about the grid x axis from +9 degrees to -24 degrees without winds and +16 degrees to -26 degrees with winds. These differences in reported mean wave direction values indicates more variation occurred in mean wave direction outputs with winds than without because the wind directions directly influenced the wave direction, whereas without winds the waves were only influenced by wave direction at the boundary and the wave bottom interactions, (Table 4.5 and Table 4.6). However, even though the values for mean wave direction

vary with and without winds, the differences in spectral methods with and without winds are similar.

At the boundary with and without winds, the RMSE values for mean direction, which quantify differences between spectral methods, ranged from about 25 to 85 degrees. The boundary also had the greatest difference between spectral methods with and without winds, as the differences in direction space of the input spectra were still preserved. The RMSE values decreased from the boundary to the nearshore for both with and without winds. In the nearshore, the RMSE values ranged from 1.6 degrees to 13.8 degrees without winds and from 1.9 degrees to 14.1 degrees with winds. Without winds in the nearshore, the waves began to turn towards shore normal as the waves interacted with the bottom contours, creating fewer differences between spectra, and with winds, the differences were lessened because the winds began to dominate the direction. The greatest spectral differences or the highest RMSE values with and without winds occurred between J Cos^2 and F MEM for all locations. As previously discussed these spectra are very different in both directional and frequency space. Spectra that were more alike in directional space had better agreement than those that did not. So, F MEM had the least differences with F MLM; and J Cos^2, J Cos^{2s}, and F LH had similar agreement. F LH, J Cos^2, and J Cos^{2s} spread energy broadly about the mean wave direction, which contributes towards their similarity in mean wave direction. F MLM and F MEM spread energy much more narrowly about the mean wave direction.

The bias indicates trends of producing bigger and smaller mean directions for each spectrum. For mean wave direction, the bias showed that J Cos^2 outputs smaller values with winds than without winds, with no other clear trends for the other spectra

(Table 4.5 and Table 4.6). The Pearson correlation values which indicate linear relationships between values were greatest in the nearshore, with winds giving higher correlation values than without winds because the winds dominate and create convergence amongst the spectra.

Table 4.5 Mean Wave Direction (deg) without winds

	Mean	RMSE	Bias	Corr	RMSE	Bias	Corr	RMSE	Bias	Corr	RMSE	Bias	Corr	RMSE	Bias	Corr
Boundary		J Cos2			J Cos2s			F LH			F MLM			F MEM		
J Cos2	9.2				32.83	-1.86	0.99	80.15	10.67	1.06	81.81	-10.13	0.93	84.78	-13.27	0.92
J Cos2S	5.3	32.83	1.86	1.01				47.53	14.39	1.04	46.40	-6.15	0.98	51.00	-9.55	0.97
F LH	19.7	80.15	-10.67	0.88	47.53	-14.39	0.83				24.69	-20.49	0.76	40.10	-24.21	0.73
F MLM	359.2	81.81	10.13	0.99	46.40	6.15	1.00	24.69	20.49	0.99				25.84	-3.79	1.00
F MEM	355.5	84.78	13.27	0.96	51.00	9.55	0.97	40.10	24.21	0.95	25.84	3.79	0.99			
Barrier Island		J Cos2			J Cos2s			F LH			F MLM			F MEM		
J Cos2	354.9				10.14	-2.01	1.01	11.15	-1.75	1.01	11.23	-1.55	1.01	11.03	-2.01	1.01
J Cos2S	353.0	10.14	2.01	1.00				3.40	0.23	1.00	3.36	0.44	1.00	3.38	-0.02	1.00
F LH	353.2	11.15	1.75	1.00	3.40	-0.23	1.00				1.14	0.20	1.00	1.88	-0.26	1.00
F MLM	353.4	11.23	1.55	1.00	3.36	-0.44	1.00	1.14	-0.20	1.00				1.54	-0.46	1.00
F MEM	352.9	11.03	2.01	1.00	3.38	0.02	1.00	1.88	0.26	1.00	1.54	0.46	1.00			
Nearshore		J Cos2			J Cos2s			F LH			F MLM			F MEM		
J Cos2	339.7				13.79	-3.12	1.00	12.88	-2.66	1.03	12.41	-1.63	1.02	12.86	-3.20	1.04
J Cos2S	336.6	13.79	3.12	1.00				2.20	0.48	0.99	2.67	1.51	0.98	1.85	-0.06	1.00
F LH	337.1	12.88	2.66	1.00	2.20	-0.48	1.00				2.05	1.03	0.99	1.62	-0.53	1.00
F MLM	338.1	12.41	1.63	1.01	2.67	-1.51	1.01	2.05	-1.03	1.01				2.02	-1.57	1.02
F MEM	336.5	12.86	3.20	0.99	1.85	0.06	0.99	1.62	0.53	0.99	2.02	1.57	0.98			

Mean, RMSE, Bias, and the Pearson correlation coefficient between mean wave direction outputs without winds

Table 4.6 Mean Wave Direction (deg) with winds

	Mean	RMSE	Bias	Corr	RMSE	Bias	Corr	RMSE	Bias	Corr	RMSE	Bias	Corr	RMSE	Bias	Corr
Boundary		J Cos2			J Cos2s			F LH			F MLM			F MEM		
J Cos2	4.5				37.03	0.22	1.00	80.75	15.60	1.05	82.25	-5.93	0.97	85.25	-9.38	0.97
J Cos2S	2.9	37.03	-0.22	1.00				47.37	15.79	1.04	45.52	-5.53	0.98	49.85	-8.86	0.98
F LH	16.4	80.75	-15.60	0.83	47.37	-15.79	0.82				25.13	-21.28	0.75	41.77	-24.72	0.73
F MLM	357.7	82.25	5.93	0.99	45.52	5.53	0.99	25.13	21.28	0.98				26.73	-3.57	1.00
F MEM	354.8	85.25	9.38	0.97	49.85	8.86	0.97	41.77	24.72	0.94	26.73	3.57	0.99			
Barrier Island		J Cos2			J Cos2s			F LH			F MLM			F MEM		
J Cos2	343.5				27.28	6.64	0.98	31.32	7.72	0.97	31.27	7.24	0.97	32.98	8.13	0.97
J Cos2S	345.9	27.28	-6.64	1.00				11.05	0.69	1.00	11.13	0.23	1.00	12.03	1.04	1.00
F LH	348.0	31.32	-7.72	1.00	11.05	-0.69	1.00				4.18	-0.45	1.00	3.48	0.34	1.00
F MLM	347.2	31.27	-7.24	1.00	11.13	-0.23	1.00	4.18	0.45	1.00				4.69	0.79	1.00
F MEM	347.8	32.98	-8.13	1.00	12.03	-1.04	1.00	3.48	-0.34	1.00	4.69	-0.79	1.00			
Nearshore		J Cos2			J Cos2s			F LH			F MLM			F MEM		
J Cos2	334.4				12.06	0.12	1.00	13.22	1.30	0.98	13.18	1.31	0.99	14.06	1.21	0.98
J Cos2S	334.5	12.06	-0.12	1.00				5.38	1.18	0.99	4.96	1.19	0.99	5.56	1.09	0.99
F LH	335.6	13.22	-1.30	1.00	5.38	-1.18	1.00				3.71	0.00	1.00	1.92	-0.09	1.00
F MLM	335.7	13.18	-1.31	1.00	4.96	-1.19	1.00	3.71	0.00	1.00				3.93	-0.09	1.00
F MEM	335.8	14.06	-1.21	1.00	5.56	-1.09	1.00	1.92	0.09	1.00	3.93	0.09	1.00			

Mean, RMSE, Bias, and the Pearson correlation coefficient between mean wave direction outputs without winds

Figures 4.7-4.9 show the differences in mean wave direction with and without winds at the three output points within the STWAVE domain. At the boundary, the direction of the waves with and without winds ranged from ± 50 degrees (figure 4.7). These directions are relative to the STWAVE grid x-axis (0 degree). In a polar coordinate system, these directions correspond with 66 to 166 degrees, or waves heading towards the northeast and the west-northwest.

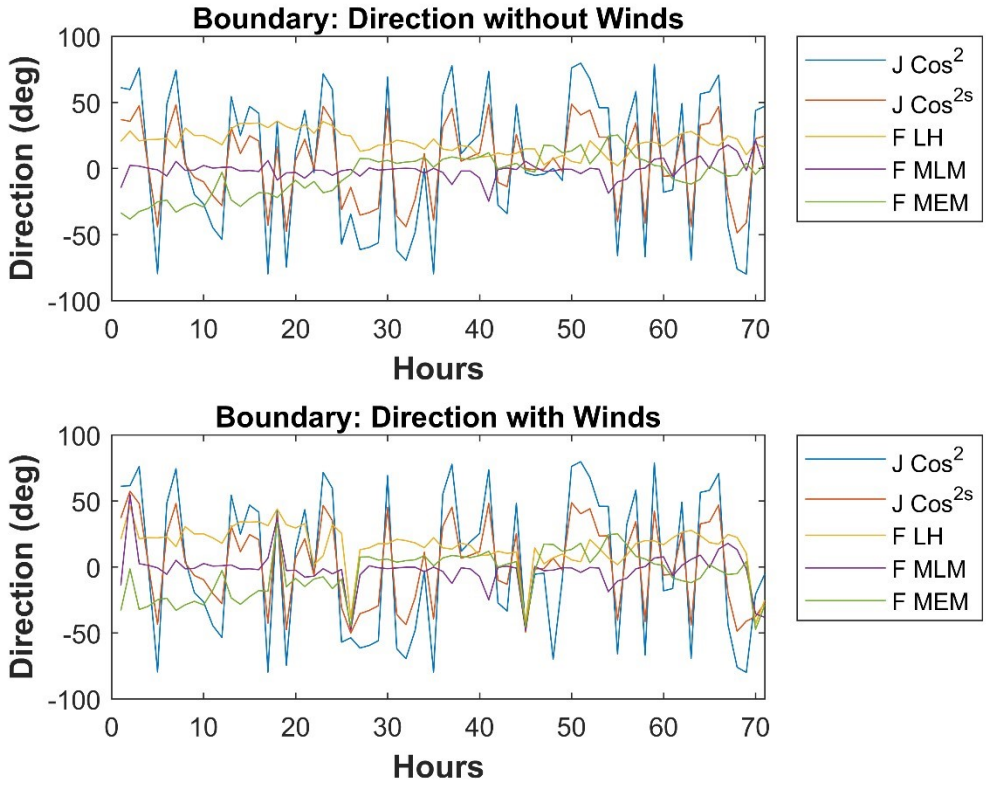

Figure 4.7 Time series of mean wave direction at the boundary point with and without winds

At the barrier island, the effect of the winds on direction were observed (figure 4.8). With winds applied, all of the spectra ranged ± 50 degrees about the x-axis, whereas without winds, the mean directions were not uniform and ranged -20 to 50 degrees about the x-axis.

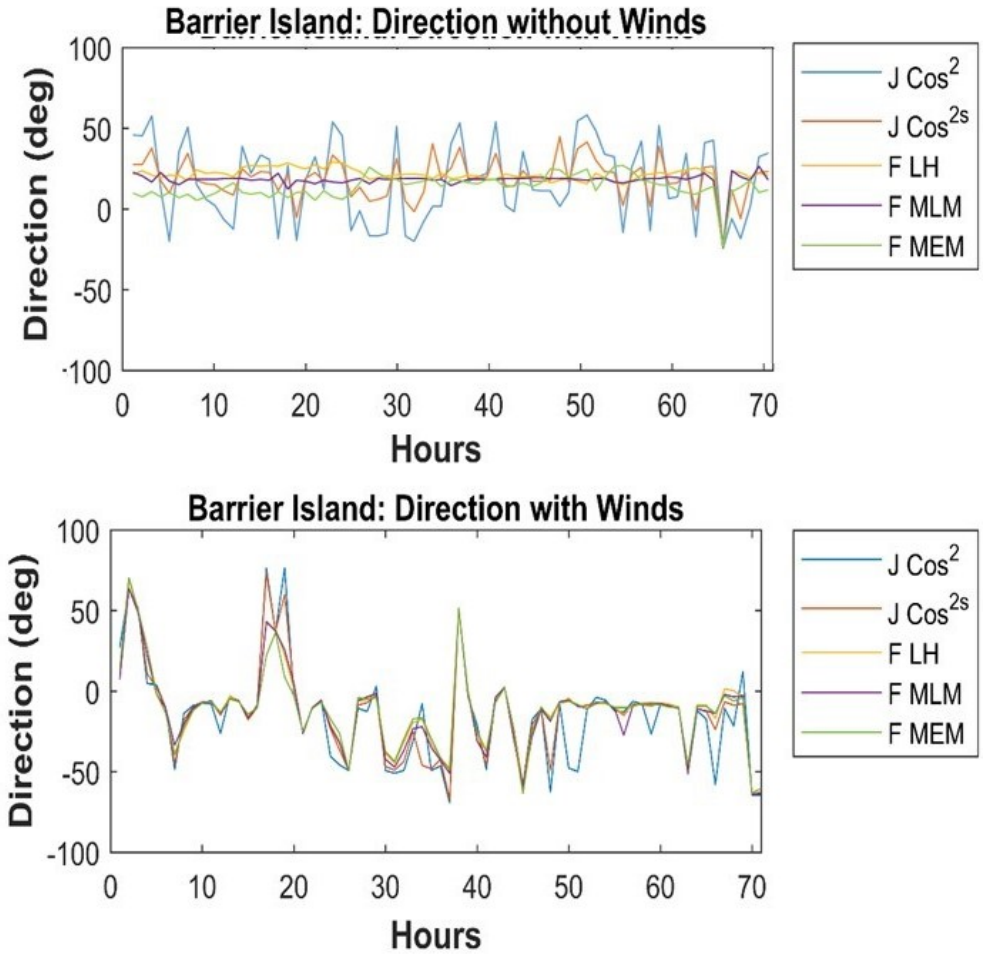

Figure 4.8 Time series of mean wave direction at the barrier island point with and without winds

In the nearshore, the direction without winds was similar between all spectral methods except J Cos^2. The direction was about 91 degrees in the polar coordinate system, which means the waves were headed shore normal towards Deer Island within Mississippi Sound (figure 4.9). J Cos^2 ranged to zero degrees, which also occurred when the wave heights and periods were zero as well. This occurred because this spectrum had frequent energy losses in the input due to truncation and then, without winds, the waves did not reach the nearshore (due to waves being directed away from the nearshore, refraction or dissipation). The direction, with winds, showed greater similarity between the spectral methods with very few observed differences between the spectral methods. There are fewer differences with winds because the wind direction dominates the waves in the nearshore.

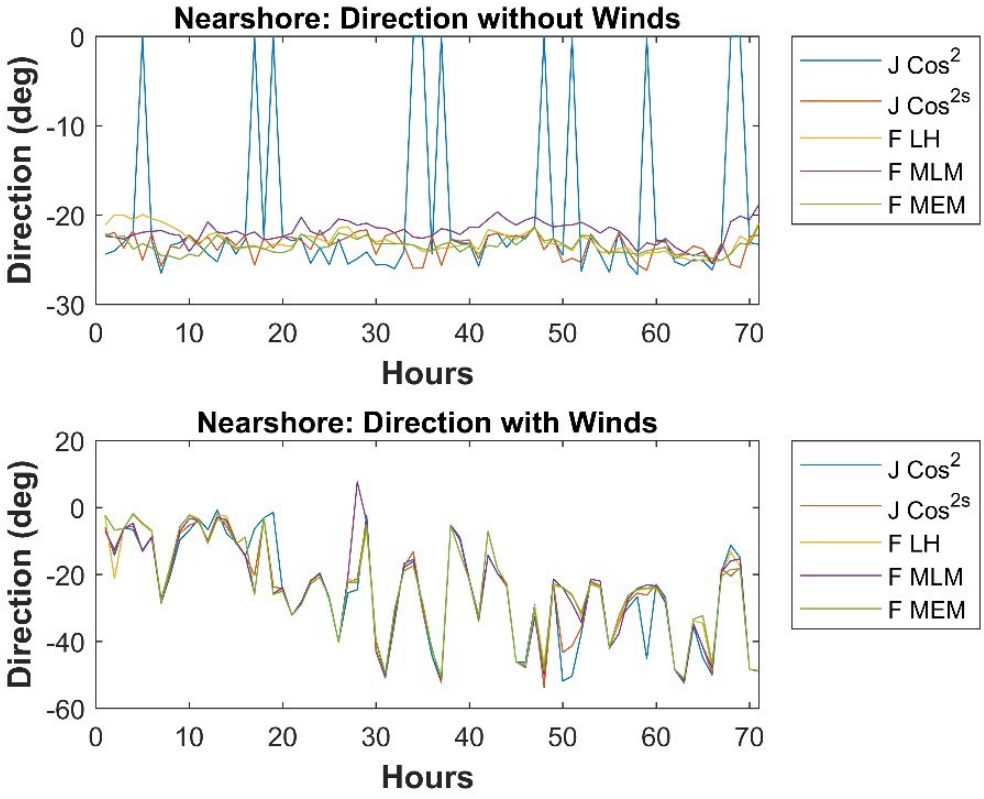

Figure 4.9 Time series of mean wave direction at the nearshore point with and without winds

CHAPTER V

CONCLUSION

This study investigated how five directional wave spectra formulations performed within the nearshore spectral wave model, STWAVE. To accomplish this task, STWAVE was run five times in half-plane mode. Each experimental run contained a different directional wave spectral formulation, a bathymetry grid, and a constant bottom friction value. These runs were performed without winds or tides, with a ± 0.5 m water elevation to simulate the diurnal tide, and with spatially constant winds.

Some assumptions made in the modeling include constant winds across the model domain, as well as no wave modification between the buoy and model domain boundary. The constant winds used within STWAVE are appropriate as the spatial scale is small, on the order of kilometers. The lack of wave modification between the buoy and the model domain is also reasonable as the depth is such that no depth-induced wave transformation would occur. Also, a single low friction factor was used over the whole model domain and no currents were applied. The constant low friction factor and the lack of applied currents is reasonable, due to the lack of gross changes in bottom friction which would seriously affect wave propagation, and the fact that the area does produce strong enough currents to affect wave propagation.

Overall, the results showed that each spectrum handled the nearshore transformation processes similarly. The wave heights and peak periods decreased towards

the nearshore and the mean wave direction turned shore normal (when not dominated by winds). Sheltering at the nearshore, due to the barrier islands was also observed with the reduction in period and wave height for the nearshore region.

Between significant wave height and peak period outputs, significant wave height contained the most differences between spectral methods with differences of up to 102%, while peak period had a maximum difference of 39%. Significant wave height was more affected by differences in the spectral methods, because it is an integration of the total power in the spectrum and thus has a greater probability to produce different values due to changes in any part of the spectrum. While the peak period is less affected by differences than wave height, it is only affected by changes to the frequency band containing the greatest amount of energy. Also, for wave height and peak period outputs, similarly produced directional spectra performed more alike than non-similarly produced directional spectra. Thus, J Cos^2 and J Cos^{2s} showed more similarities in outputs, than with the FFT generated spectra. J Cos^2 and J Cos^{2s} spectra also tended to give the maximum integral parameter differences observed between the spectral methods, particularly J Cos^2. J Cos^2 produces these greater differences because of the potential for the Cos^2 spreading function to cause spectral energy losses from truncation for mean wave directions headed away from the grid x axis.

The mean wave direction showed greater variability on the boundary but showed more uniformity in the nearshore either due to the influence of winds or the influence of the bottom contours. Also, for mean wave direction outputs, the spreading functions seemed to determine differences based on spread in direction space. Meaning broadly spread spectra performed more similarly than with outputs of narrowly spread spectra.

The broadly spread spectra were F LH, J Cos^2 and J Cos^{2s}. The narrowly spread spectra were F MLM and F MEM.

Without winds, the spectral differences were apparent from the boundary to the nearshore. Wave height showed the same differences produced at the boundary were still present in the nearshore, this was reflected in the increasing percent difference (24%-48% at boundary, 37-64% at nearshore). Peak period showed an increase in differences at the nearshore when compared to the boundary because of the differences in energy placement in the frequency bands (9-11% at the boundary to 20-34% at the nearshore). The mean wave direction showed more uniformity in the nearshore than at the boundary due to the influence of bottom contours.

The inclusion of winds resulted in differences in the values of each wave parameter and in the differences between spectral methods compared to no winds. The overall energy levels were greater with winds than without wind. Differences between wave parameters for the different spectral methods with winds at the boundary were similar to the differences observed at the boundary without winds. However, at the barrier island and nearshore regions, the winds began to dominate the wave field and cause more uniformity between spectra outputs. The influence of the wind was evident in the percent difference statistic of 51-96% at boundary, 38-63% in nearshore for wave heights and 7-11% at the boundary to 17%-38% in the nearshore for peak period. The boundary is not as affected by the winds as the other locations because the winds have not blown over a great enough fetch within the model domain in order to influence the outputs.

The addition of the water elevation adjustments to simulate the tide resulted in slight differences in values of wave height and period, but it did not cause any changes in the differences between spectral methods applied at the offshore boundary, indicating that small water level variations are not a concern when specifying the offshore boundary spectra.

In conclusion, all five spectral methods performed appropriately within the nearshore wave model, as all of the spectra outputs showed the nearshore transformation processes. However, each spectral method did produce different wave parameters within STWAVE, even though they were all created using the same buoy input data. J Cos^2 produced the most divergent outputs, which is due to the occurrence of energy losses in the spectra when the mean wave direction was headed outside of the model grid.

Overall, the greatest differences between spectral methods were observed in the significant wave height parameter with difference of up to 105% without winds and 102% with winds when using a parametric function. Meaning significant differences between spectra can occur depending on the chosen boundary spectral computation method. The mean wave direction showed greater differences at the boundary and less difference as the wave enters the nearshore. The peak period had fewer differences at the boundary and barrier islands, but at the nearshore the differences between spectra were increased by 10% for both with and without winds, however the Pearson correlation values were significantly altered by the winds with values from approximately 0.60 to 0.90 with winds and 0.05 to 0.60 without winds.

Winds had a significant impact on observed differences between the spectra. Differences in wave height that were observed at the barrier islands and nearshore

without winds were no longer observed when winds were present. Thus, if winds are applied, the use of any directional wave spectra formulation is comparable at the nearshore for this barrier island sheltered location.

Therefore, in response to Earle et al. (1999)'s conclusions on determining the best method to use with a model, for the use of STWAVE in a low energy, shallow, and sheltered environment like the Mississippi sound, if winds are applied, any of the directional wave spectra methods can be used as the winds will create uniformity between the methods. However, without winds, additional validation is needed to determine which spectra outputs within the model wave parameters best agrees with measured nearshore data, and thus conclude a best method. The results also indicate that less parametric methods are better if the needed information is available to quantify them. If not, an awareness of the mean wave direction and the correlating spectral energy losses as a result of using the parametric equations need to be considered. The results show that both available information to produce the spectra, as well as, site conditions like local winds and depth, affect the usefulness of each spectral technique.

In future work, a repetition of this study in a location with higher wave energy would be of interest, to determine the effect overall energy in the system has on each spectral method performance. Also, an understanding of which spectral method provides the best match to the conditions that evolve in the nearshore would be useful without winds. Likewise, a method of statistically analyzing differences between spectra without using the integral parameters could prove useful in determining the effectiveness of each method.

REFERENCES

Ahsan, Q., Barron, C., Blaha, J., Blumberg, A., Fitzpatrick, P., Herndon, D., Herring, H., Hsu, Y., Keen, T., Li, H., Li, Y., Patchen, R., Szczechowski, C., Willems, R., and Wilz, P. (2002) Northern Gulf of Mexico Littoral Initiative Modeling Program. Estuarine and Coastal Modeling (2001): pp. 949-965

Ahsan, Q., Blumberg, A. F., Li, H., & Blaha, J. (2002, October). The calibration/validation of a Mississippi Sound/Bight model. In OCEANS'02 MTS/IEEE (Vol. 2, pp. 823-833). IEEE.

Blumberg, A. F., Ahsan, Q., & Lewis, J. K. (2000). Modeling hydrodynamics of the Mississippi Sound and adjoining rivers, bays and shelf waters. In OCEANS 2000 MTS/IEEE Conference and Exhibition (Vol. 3, pp. 1983-1989). IEEE.

Booij, N., Ris, R. C., & Holthuijsen, L. H. (1999). A third-generation wave model for coastal regions: 1. Model description and validation. Journal of geophysical research: Oceans, 104(C4), 7649-7666.

Bouws, E., Günther, H., Rosenthal, W., & Vincent, C. L. (1985). Similarity of the wind wave spectrum in finite depth water: 1. Spectral form. Journal of Geophysical Research: Oceans, 90(C1), 975-986.

Bretherton, F. P., & Garret, C. I. R. (1970). Wavetrains in inhomogeneous moving media. In Hyperbolic Equations and Waves (pp. 211-236). Springer Berlin Heidelberg.

Brissette, F. P., & Tsanis, I. K. (1994). Estimation of wave directional spectra from pitch-roll buoy data. Journal of waterway, port, coastal, and ocean engineering, 120(1), 93-115.

Bunya, S., Dietrich, J. C., Westerink, J. J., Ebersole, B. A., Smith, J. M., Atkinson, J. H., ... & Cardone, V. J. (2010). A high-resolution coupled riverine flow, tide, wind, wind wave, and storm surge model for southern Louisiana and Mississippi. Part I: Model development and validation. Monthly Weather Review, 138(2), 345-377.

Cartwright, D.E., 1963. The use of directional spectra in studying the output of a wave recorder on a moving ship. In: Ocean Wave Spectra. Prentice Hall, New York, pp. 203–219.

Capon, J. (1969). "High-resolution frequency-wavenumber spectrum analysis." Proc. IEEE, 57, 1408-1418

Demirbilek, Z., & Panchang, V. (1998). CGWAVE: A coastal surface water wave model of the mild slope equation (No. TR-CHL-98-26). ARMY ENGINEER WATERWAYS EXPERIMENT STATION VICKSBURG MS.

Earle, M. D. (1996). Nondirectional and directional wave data analysis procedures. NDBC technical Document, 96001.

Eleuterius, Charles K., and Sheree L. Beaugez. 1979. Mississippi Sound: A Hydrographic and Climatic Atlas. Physical Oceanography Section, Gulf Coast Research Laboratory, Ocean Springs, Mississippi for Mississippi-Alabama Sea Grant Consortium: MASGP-79-009. Page 16 (135pp).

Goda, Y., 1985. Random seas and design of maritime structures. University of Tokyo press.

Goda, Y. (1999). A comparative review on the functional forms of directional wave spectrum. Coastal Engineering Journal, 41(01), 1-20.

Gonçalves, M., Rusu, E., & Soares, C. G. (2012). Evaluation of the wave models SWAN and STWAVE in shallow water using nested schemes. Maritime Engineering and Technology, 481.

Hashimoto, N., Nagai, T., & Asai, T. (1995). Extension of the maximum entropy principle method for directional wave spectrum estimation. In Coastal Engineering 1994 pp. 232-246.

HASSELMANN, K. et al. (1973). Measurements of wind-wave growth and swell decay during the Joint North Sea Wave Project (JONSWAP). D. Hydrogr. Z. 12 (8).

Hasselmann, K., T.P. Barnett, E. Bouws, H. Carlson, D.E. Cartwright, K. Enke, J.A. Ewing, H. Gienapp, D.E. Hasselmann, P. Kruseman, A. Meerburg, P. Muller, D.J. Olbers, K. Richter, W. Sell, and H. Walden. 1973. Measurements of wind-wave growth and swell decay during the Joint North Sea Wave Project (JONSWAP). Deut. Hydrogr. Z., Suppl. A, 8(12): 1-95.

Holthuijsen, L.H. 2007. Waves in ocean and coastal waters. Cambridge: Cambridge University Press. 387 pp

Hsu, Y. L., W.E. Erick, J.M. Kaihatu, and R.A. Allard. (2000). “Application of SWAN in Mississippi Sound.” Proceedings 6th International Workshop on Wave Hindcasting and Forecasting, Monterey, CA, pp. 398-403.

Hughes, S. A. (1985). Directional wave spectra using cosine-squared and cosine 2s spreading functions. Coastal Engineering Technical Note. Coastal Engineering Research Center, Coastal and hydraulics Laboratory.

Jensen, R. E. (1983). Mississippi Sound wave-hindcast study : main text and appendices A and B. Mobile, Ala. : The District ; Vicksburg, Miss. : US Army Corps of Engineers, Hydraulics Laboratory, [1983].

Kaihatu, J. M., Rogers, W. E., Hsu, Y. L., & O'Reilly, W. C. (1998). Use of phase-resolving numerical wave models in coastal areas (No. NRL/PP/7322--97-0042). NAVAL RESEARCH LAB STENNIS SPACE CENTER MS COASTAL AND SEMI-ENCLOSED SEAS SECTION.

Kitaigordskii, S. A., Krasitskii, V. P., & Zaslavskii, M. M. (1975). On Phillips' theory of equilibrium range in the spectra of wind-generated gravity waves. Journal of Physical Oceanography, 5(3), 410-420.

Kumar, V. S., Deo, M. C., Anand, N. M., & Kumar, K. A. (2000). Directional spread parameter at intermediate water depth. Ocean engineering, 27(8), 889-905.

Long, R. B. 1980. "The Statistical Evaluation of Directional Spectrum Estimates Derived from Pitch/Roll Buoy Data," Journal of Physical Oceanography, Vol 10, pp. 944.

Longuet-Higgins, M. S., Cartwright, D. E., and Smith, N. D. (1963). "Observations of the directional spectrum of sea waves using the motions of a floating buoy." Ocean Wave Spectra, Prentice-Hall, Englewood Cliffs, N.J., 111-132.

Longuet-Higgins, M.S., Cartwright, D.E., and Smith, N.D., (1963), "Observations of the directional spectrum of sea waves using the motions of a floating buoy," Ocean Wave Spectra, Prentice-Hall, Englewood Cliffs, NJ.

LONGUET-HIGOINS M. S., D. E. CARTWRIGHT and N. D. SMITH (1963) Observations of the directional spectrum of sea waves using the motions of a floating buoy. In: Ocean wave spectra, Prentice-Hall, Englewood Cliffs, New Jersey, pp. 111-136.

Lygre, A., and Krogstad, H. E. (1986). "Maximum entropy estimation of the directional distribution in ocean wave spectra." J. Phys. Oceanogr., 16, 2052-2060.

Massey, T. C., Anderson, M. E., Smith, J. M., Gomez, J., & Jones, R. (2011). STWAVE: Steady-state spectral wave model user's manual for STWAVE, Version 6.0 (No. ERDC/CHL-SR-11-1). ENGINEER RESEARCH AND DEVELOPMENT CENTER VICKSBURG MS COASTAL AND HYDRAULICS LAB.

Mitsuyasu, H., Tasai, F., Suhara, T., Mizuno, S., Ohkusu, M., Honda, T., Rikiishi, K., 1975. Observations of the directional spectrum of ocean waves using a cloverleaf buoy. Journal of Physical Oceanography 5, 750–760.

Memos, C. D., & Tsiachris, A. (2001). Wave Directionality In Shallow Water. WIT Transactions on The Built Environment, 58.

NortekAS. (2002, December 15). Wave Measurements using the PUV method. Retrieved November 11, 2016, from http://www.nortek-as.com/lib/technical-notes/puv-wave-measurement/view

Nwogu, O. (1989). Maximum entropy estimation of directional wave spectra from an array of wave probes. Applied Ocean Research, 11(4), 176-182.

Outlaw, D. G. (1983). Prototype tidal data analysis for Mississippi Sound and adjacent areas. Vicksburg, Miss. U.S. Army Engineer Waterways Experiment Station; Springfield, Va.: Available from National Technical Information Service, 1983.

Panicker, N. N., & Borgman, L. E. (1970). Directional spectra from wave-gage arrays. In Coastal Engineering 1970 (pp. 117-136).

Pierson, W. J., and L. Moskowitz, 1964: A proposed spectral form for fully developed wind seas based on the similarity theory of A. A. Kitaigorodskii. J. Geophys. Res., 69, 5181–5190.

Portilla-Yandun, J., & Cavaleri, L. (2016). On the specification of background differences for wave data assimilation systems. Journal Of Geophysical Research: Oceans, 121(1), 209-223. doi:10.1002/2015JC011309

Ris, R. C., Holthuijsen, L. H., & Booij, N. (1999). A third-generation wave model for coastal regions: 2. Verification. Journal of Geophysical Research: Oceans, 104(C4), 7667-7681.

Rusu, E., & Soares, C. G. (2009). Validation of two wave and nearshore current models. Journal of waterway, port, coastal, and ocean engineering, 136(1), 27-45.

Rusu, E., Gonçalves, M., & Soares, C. G. (2011). Evaluation of the wave transformation in an open bay with two spectral models. Ocean engineering, 38(16), 1763-1781.

Sheng, Y. and Butler, H. (1982) Modeling Coastal Currents and Sediment Transport. Coastal Engineering 1982: pp. 1127-1148.

Siadatmousavi, S. M., Jose, F., & Miot da Silva, G. (2016). Sensitivity of a third generation wave model to wind and boundary condition sources and model physics; a case study from the South Atlantic Ocean off Brazil coast. Computers & Geosciences, 90(Part B), 57-65. doi:10.1016/j.cageo.2015.09.025

Slinn, D. (2008). Wave Setup Methodology for the Fema Mississippi Flood Study. Technical Report, Federal Emergency Management Agency.

Smith, J. M. (2007). Modeling nearshore waves for Hurricane Katrina (No. ERDC-TN-SWWRP-07-6). ENGINEER RESEARCH AND DEVELOPMENT CENTER VICKSBURG MS.

Smith, J. M. (2001). Modeling nearshore wave transformation with STWAVE (No. ERDC/CHL CHETN-I-64). ENGINEER RESEARCH AND DEVELOPMENT CENTER VICKSBURG MS COASTAL AND HYDRAULICS LAB.

Smith, J.M., Sherlock, A. R., Resio, D.T. (2001). "STWAVE: Steady-state spectral wave model user's manual for STWAVE Version 3.0," CE-ERDC/CHL SR-01-1, U.S. Army Engineer Research and Development Center, Vicksburg, MS

Sorensen, R. M. (2005). Basic coastal engineering (Vol. 10). Springer Science & Business Media.

Steele, K. E., Teng, C. C., & Wang, D. W. C. (1992). Wave direction measurements using pitch-roll buoys. Ocean Engineering, 19(4), 349-375.

Van der Westhuysen, A. (2012). Modeling nearshore wave processes. In ECWMF Workshop on "Ocean Waves", European Centre for medium-range weather forecasts, Reading.

van Vledder, G., Zijlema, M., & Holthuijsen, L. (2011). Revisiting the JONSWAP bottom friction formulation. Coastal Engineering Proceedings, 1(32), 41.

Veeramony, J., M.D. Orzech, K.L. Edwards, M. Gilligan, J. Choi, E. Terrill, and T. De Paolo. (2014). Navy nearshore ocean prediction systems. Oceanography 27(3):80–91, http://dx.doi.org/10.5670/oceanog.2014.70.

Waals, O. J., Aalbers, A. B., & Pinkster, J. A. (2002). Maximum likelihood method as a means to estimate the directional wave spectrum and the mean wave drift force on a dynamically positioned vessel. Proceedings of OMAE2002, Oslo, Norway.

Wamsley, T. V., Godsey, E. S., Bunch, B. W., Chapman, R. S., Gravens, M. B., Grzegorzewski, A. S., ... & Tillman, D. L. (2013). Mississippi Coastal Improvements Program; Evaluation of Barrier Island Restoration Efforts (No. ERDC-TR-13-12). ENGINEER RESEARCH AND DEVELOPMENT CENTER VICKSBURG MS COASTAL AND HYDRAULICS LAB.

Wang, D.W., 1992. Estimation of wave directional spreading in severe seas. Proceedings of the Second International Offshore and Polar Engineering Conference, III, pp. 146–153.

APPENDIX A

TERMS AND EQUATIONS

A.1 Wave Parameters

Wind waves are typically reported by their height, period, and direction. Wind waves are comprised of a wavelength, a wave period, and an amplitude (figure A.1). The wavelength is the span between two wave crests and the wave height is equal to twice the amplitude. The wave period, not shown in figure A.1, is defined as the time between two successive crests. These parameters can either be found from field data in a time series or through spectral analysis.

The height of the wave can be measured by the eye or through a device, such as a buoy. For engineering purposes, the larger wave heights in a time series are of interest. To capsulate these higher values, a statistical estimation known as the significant wave height is used. The significant wave height can be determined in two ways. The first is through the average of the tallest third waves in a time series and the second is through the use of the frequency spectrum, as shown in the following equation:

$$H_{m0} = 3.8\sqrt{m_0} \tag{A.1}$$

Where, H_{m0} (m) is the significant wave height and m_0 (m2/Hz) is the integral of the frequency spectrum. The frequency spectrum is a one dimensional function of wave energy and frequency, with frequency being the inverse of the wave period.

The wave period can be determined by timing wave crests as they pass a fixed position or through taking the inverse of the wave frequency. The wave period can also be reported as either the peak period (T_p) or the mean period (T_m). The spectral peak period is associated with the highest peak in the frequency spectrum or the frequency

with the greatest amount of energy, and the spectral mean period is defined by the average of all periods as shown below:

$$T_{m02} = \sqrt{\frac{m_0}{m_2}} \tag{A.2}$$

Where, T_{m02} (sec) is the mean period, m_0 (m^2) is the zero moment and m_2 (m^2) is the second moment of the frequency spectrum (NortekAS, 2002). Where each moment k can be defined as:

$$m_k = \int f^k C(f) df \tag{A.3}$$

Where, m_k (m2) is the kth moment of the frequency spectrum, f (Hz) is the frequency, and C (m2/Hz) is the frequency spectrum (NortekAS, 2002).

Wave direction refers to the dominant direction of the wave. Wave direction can be determined from the shoreline by approximating the angle of approach, or it can be defined spectrally through a directional wave spectrum. A directional wave spectrum is the two dimensional distribution of wave energy over frequency and direction and is expressed as:

$$E(f, \theta) = S(f) D(f, \theta) \tag{A.4}$$

Where, $E(f, \theta)$ (m^2/Hz/deg) is the directional wave spectra, θ (deg) is the mean wave direction, f (Hz) is the frequency, S (m^2/Hz) is the distribution for the frequency domain and D (Hz/deg) is the normalized directional distribution.

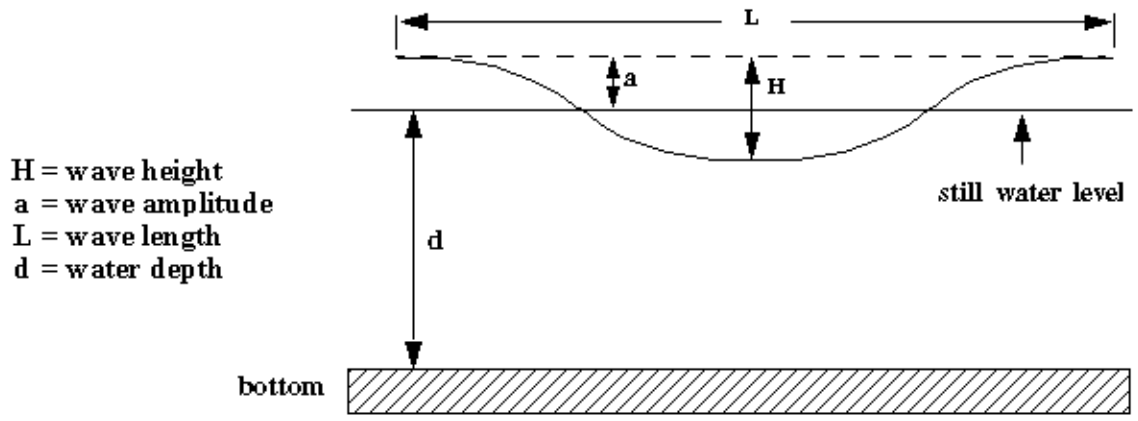

Figure A.1 Parts of a wave (Sorensen 2005)

A.2 Nearshore Transformation of Waves

Waves are made of energy moving transversely through the ocean in an almost sine-like shape which is visible from the surface. However, unseen, the energy also propagates beneath the wave to a finite depth, in a circular motion known as orbitals. When these orbitals reach a depth in which they can "feel" the bottom, they begin to interact with the ocean floor. These wave-bottom interactions are what causes the wave to transform in the nearshore. As the orbitals encounter shallower water, the celerity, or speed of the wave, begins to change. The celerity of the wave is a function of wavelength and period, as shown below:

$$C = L/T \tag{A.5}$$

Where, L is the wavelength (m), T (sec) is the period, and, C (m/s) is the celerity equal to the distance traveled by a crest per unit of time. Celerity can also be calculated through the equation of motion and the small amplitude theory (Sorensen, 2005), which requires a/L and a/d to be small, and is expressed as:

$$C = \sqrt{\frac{gL}{2\pi}\tanh(2\pi\frac{d}{L})} \quad \text{(A.6)}$$

Where, a is amplitude (m) , g is gravitational acceleration (m/s^2), L (m) is wavelength, d (m) is depth, and C (m/s) is the celerity, now a function of wavelength and relative depth (d/L).

The celerity of the wave will be dictated by this expression when the relative depth is less than 0.5 and greater than 0.05. As the wave enters shallower water, and the relative water depth reaches a ratio of less than 0.05, the hyperbolic tangent function (tanh) will roughly equal (2π)/L, resulting in the expression:

$$C = \sqrt{gd} \quad \text{(A.7)}$$

Indicating that when the wave becomes a shallow water wave, the speed is directly related to the water depth and not wave period.

Therefore, as a wave encounters decreasing water depths, the wave's celerity will also decrease. This decrease in wave speed with water depth results in a change in the wave's direction, through a processes called refraction. Refraction occurs when a portion of the wave crest encounters shallower water and begins to propagate forward at a slower speed than the portion of the wave that is still in deeper water. The result is the wave crests bends along the bathymetry contours approaching shore almost always parallel (Sorensen, 2005). This reduction in celerity can also result in changes to the wave height. When the wave slows, the period remains constant and as a result the wavelength must shorten which increases the wave's amplitude and thus its height. As the wave moves into increasingly shallower water, there will come a point when the tip of the wave or

wave crest is moving faster than the wave base. This imbalance will cause the wave crest to fall forward and break.

These transformation processes generally begin to occur at intermediate depths of 15-60 meters (Smith, 2001). However, the specific depth that transformation will begin is not the same for all waves. Waves of higher frequency do not penetrate as deeply as lower frequency waves. Hence, higher frequency waves will feel the bottom at a shallower depth than lower frequency waves within the same area. The frequency and type of wave break determines the wave climate of an area.

A.3 Directional Wave Spectra

The sea's surface is composed of many different waves with various amounts of energy moving in different directions. A directional wave spectrum is the graphic interpretation of that complex sea state in order to quantify it for any moment of time. The directional spectrum is created by transforming a frequency spectrum with a directional spreading function which spreads the energy density about the mean wave direction and is expressed as:

$$E(f,\theta) = E(f)D(\theta,f) \tag{A.8}$$

Where, E(f,θ) (m2/Hz/deg) is the directional spectrum, $E(f)$ m2/Hz) is the frequency spectrum (energy density) $D(\theta,f)$ (Hz/deg) is the directional spread function. This directional spectrum, E(f,θ), is what is used as an input into STWAVE.

There are a number of methods available to estimate both the frequency spectrum and the directional spreading function components of the directional wave spectra. The frequency spectrum differentiates each wave based on its period, and creates a one dimensional spectrum correlating wave energy with each frequency. There are several

methods available, but two of the most common methods are a JONSWAP frequency spectrum and a Fast Fourier Transformation derived frequency spectrum.

The JONSWAP frequency spectra method was defined by the experiments of the Joint North Sea Wave Project (Hasselman et al. 1973). The JONSWAP method is an expansion on the Pierson-Moskowitz function, which creates a frequency spectrum using only the significant wave height, the peak period, and the mean wave direction. It is based on an empirical relationship and is fetch limited. The JONSWAP equation is defined as:

$$S(f) = \frac{\alpha g^2}{(2\pi)^4 f^5} e^{-1.25\left(\frac{fp}{f}\right)^4} y^{\alpha} \quad \text{(A.9)}$$

Where, $S_h(f)$ is a spectrum of buoy heave motion, PTF is a power transfer function, and S_w (f) is the wave spectrum first described as acceleration and then transformed into displacement which creates the frequency spectrum. The JONSWAP frequency spectrum has some limitations as it is only an approximation of the frequency spectra and does not place much energy into the higher frequencies.

The JONSWAP method was designed for use in deep water, however a depth and frequency dependent function has been developed which can be applied to allow for use in shallow water environments, known as a TMA spectrum (Bouws et al. 1985; Sorensen 2005).

The Fast Fourier Transformation derives frequency spectra using the time series of the heave of a buoy is described in detail by Steele et al. (1992) in an NDBC briefing. The Fast Fourier Transformation technique can be expressed as:

$$S_w(f) = \frac{S_h(f)}{PTF} \quad \text{(A.10)}$$

Where, S_h (f) is a spectrum of buoy heave motion, PTF is a power transfer function, and S_w (f) is the wave spectrum first described as acceleration and then transformed into displacement which creates the frequency spectrum. The Fast Fourier Transformation method has some limitations due to the buoys being subject to errors during signal processing or sensor failure.

These two methods produce similar frequency spectra (figure A.2). However, the JONSWAP frequency spectra is generally much smoother and the Fast Fourier Transformation spectra is peaky (Figure A.2)

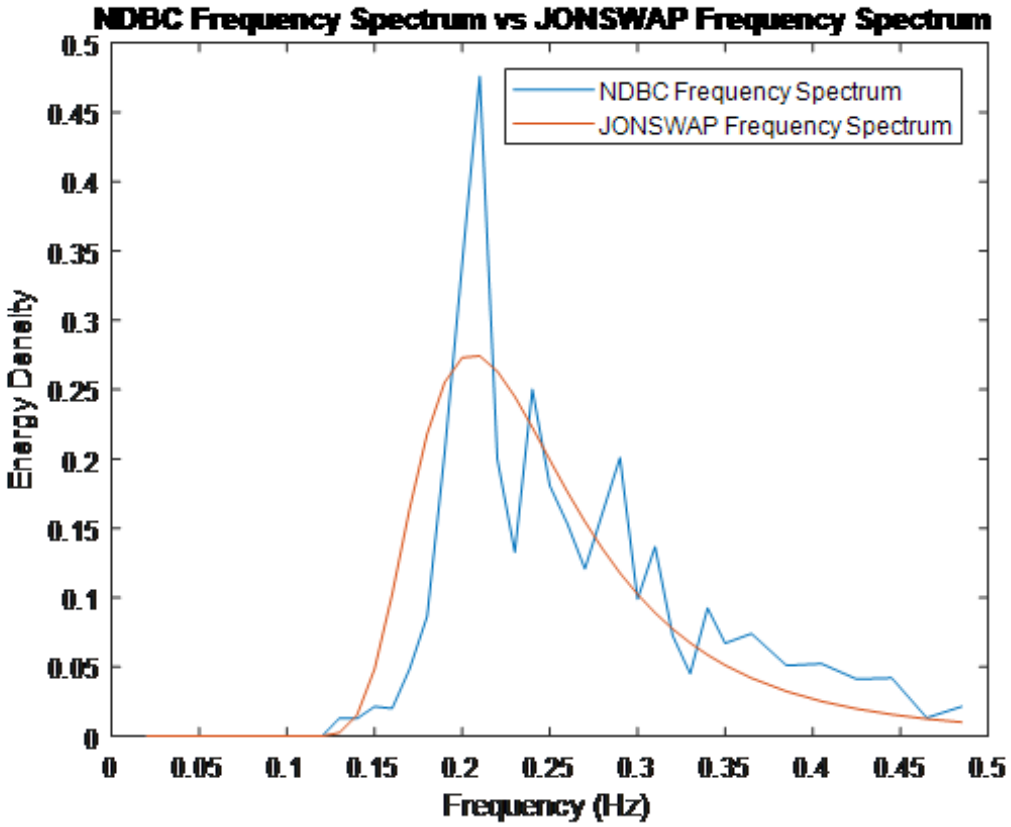

Figure A.2 Fast Fourier Transformation vs JONSWAP frequency spectra

The directional spreading functions dictate how much of the given energy density in the frequency spectrum is spread over the directional angles for each frequency band. The directional spreading functions used in this study were the Longuet-Higgins function, the maximum likelihood method, the maximum entropy method, cosine squared and cosine 2s functions. The Longuet-Higgins method, created by Longuet-Higgins et al. (1963), is the method suggested by NDBC, as it uses the Fast Fourier Transformation directional coefficients from the NDBC buoys. This function produces broad peaks with energy being well distributed around the mean wave direction (figure A.3). The function can be described as:

$$D(f,\theta) = \frac{1}{\pi}\left[\frac{1}{2} + r_1\cos(a-\alpha_1) + r_2\cos\big(2(a-\alpha_2)\big)\right] \qquad \text{(A.11)}$$

Where, r_1 and r_2 are the first and second Fourier transformation coefficients and describe directional energy spreading and α_1 and α_2 are the third and fourth coefficients and describe the mean and principal wave direction (Earle 1996).

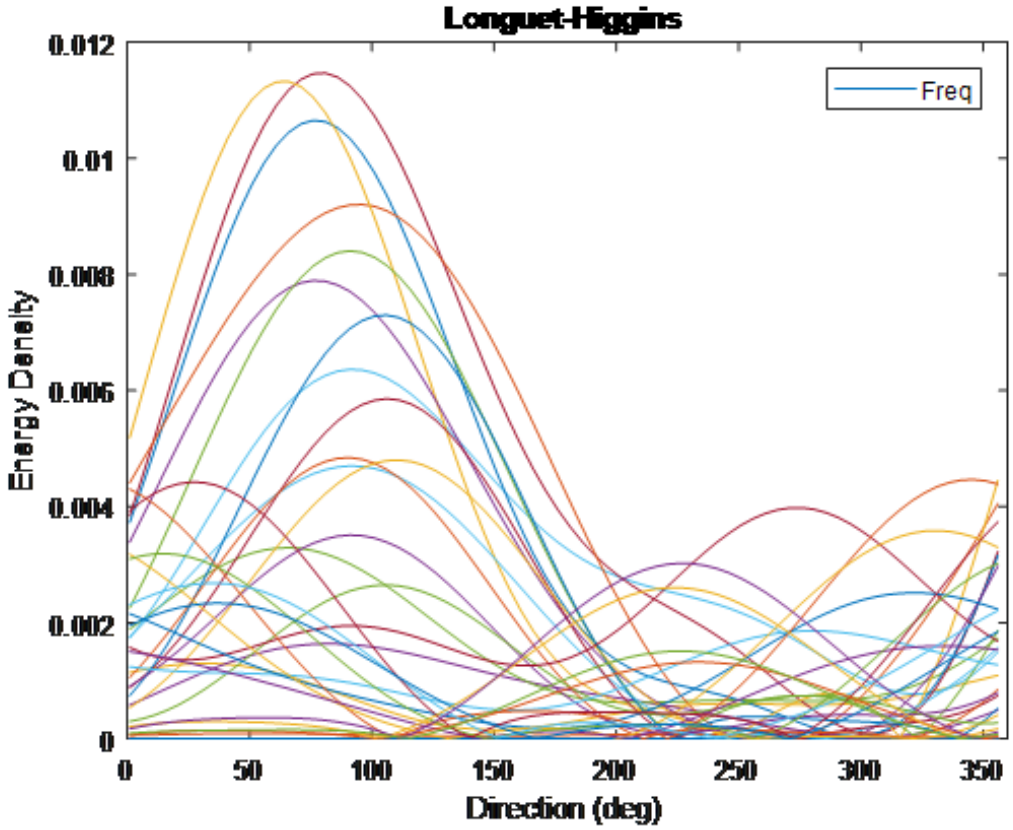

Figure A.3 Longuet-Higgins distribution

Another directional spreading function is the Maximum Likelihood Method which estimates the mean and variance for the directional spectrum, and then creates a distribution with those parameters (Capon 1969). The Maximum Likelihood Method produces a more peaked distribution than the Longuet-Higgins method (figure A.4) and can be described as:

$$D(f,\theta) = \frac{1}{2}a_0 + a1\cos(\theta) + b_1\sin(\theta) + a_2\cos(2\theta) + b_2\sin(2\theta) \qquad \text{(A.12)}$$

Where a_0,a_1,b_1,a_2,b_2 are computed using the cross spectral densities utilizing the r_1, r_2, α_1, α_2 and frequency spectra values.

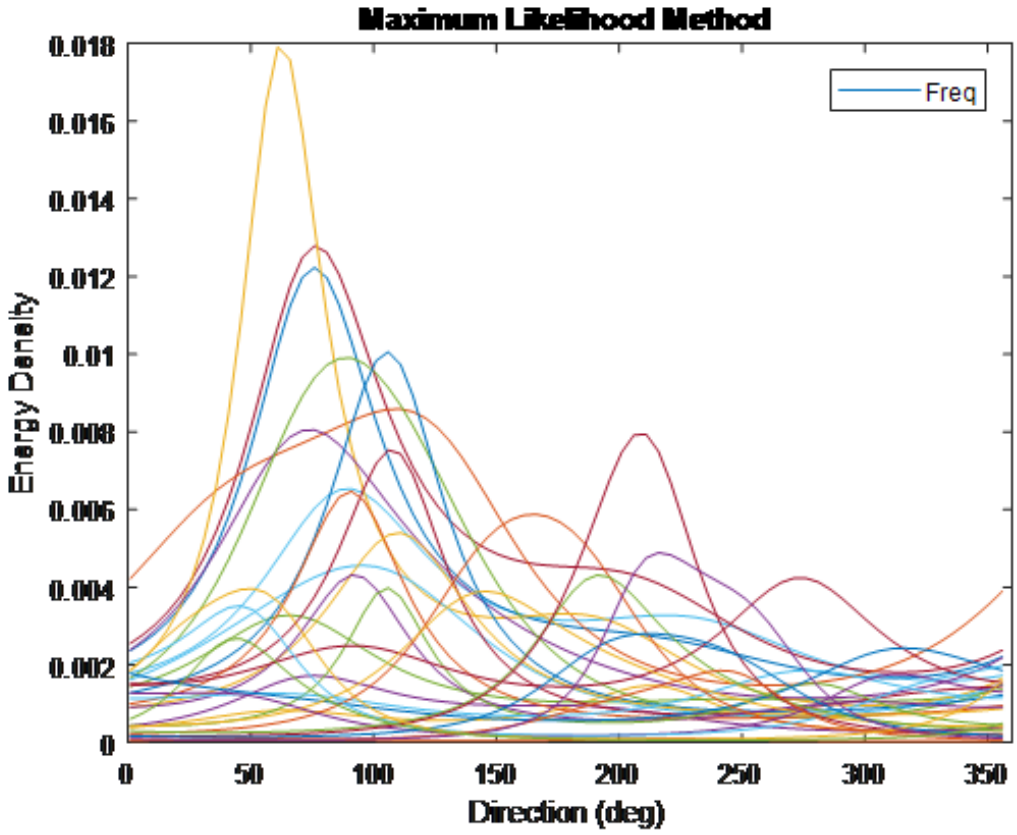

Figure A.4 Maximum Likelihood distribution

The Maximum Entropy Method has the highest directional resolving power and the narrowest peaks (figure A.5). The Maximum Entropy Method estimates the distribution with the highest entropy. It is computed using the cross spectral density matrix obtained by the Fast Fourier Transformation to estimate the directional spread for each frequency band (Lygre and Krogstad 1986), and is expressed as:

$$D(f,\theta) = \frac{1-d_1c_1-d_2c_2}{2\pi\left|1-d_1e^{-i\varphi}-d_2e^{-2i\varphi}\right|^2} \quad \text{(A.13)}$$

Where, d_1,d_2, c_1, c_2 are computed using the cross spectral densities utilizing the r_1, r_2, α_1, α_2 and frequency spectra values.

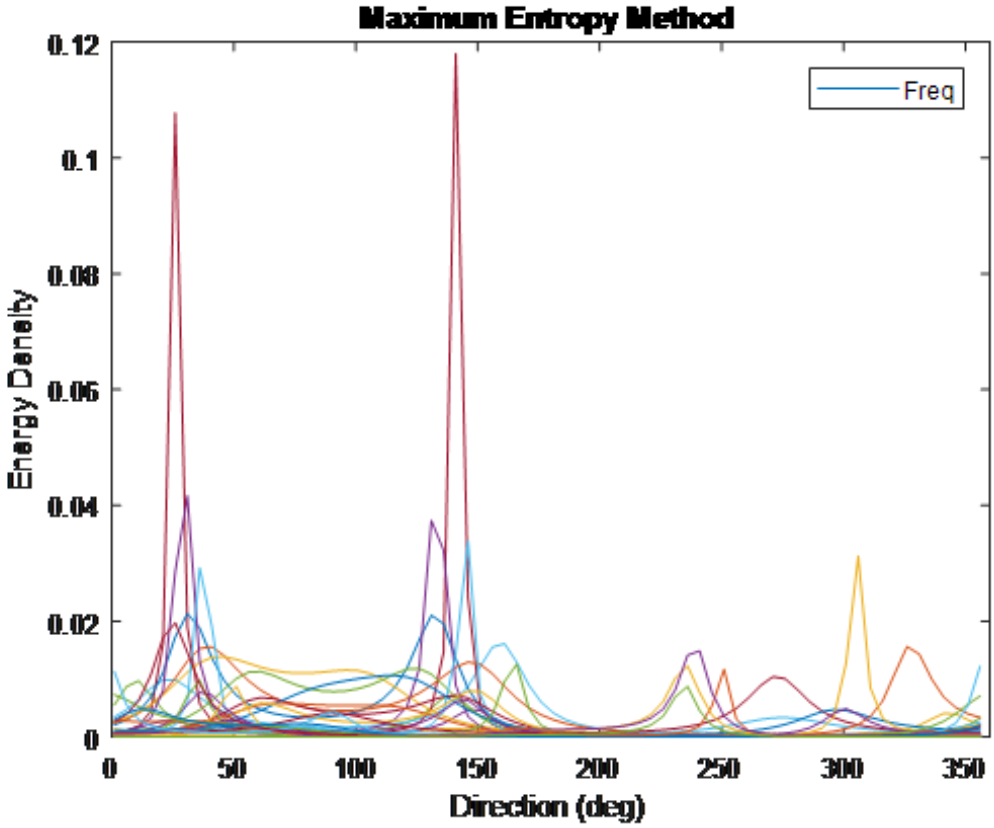

Figure A.5 Maximum Entropy distribution

Cosine squared and cosine 2s are the simplest spreading functions. Cosine squared simply takes the energy densities and spreads them around the mean wave direction in a cosine squared shape (figure A.6). This is defined as:

$$D(f,\theta) = \cos^2(\theta - \theta_m) \tag{A.14}$$

Until $\theta = \theta_m$, and then $D(f,\theta) = 0$,

Where θ_m is the mean wave direction.

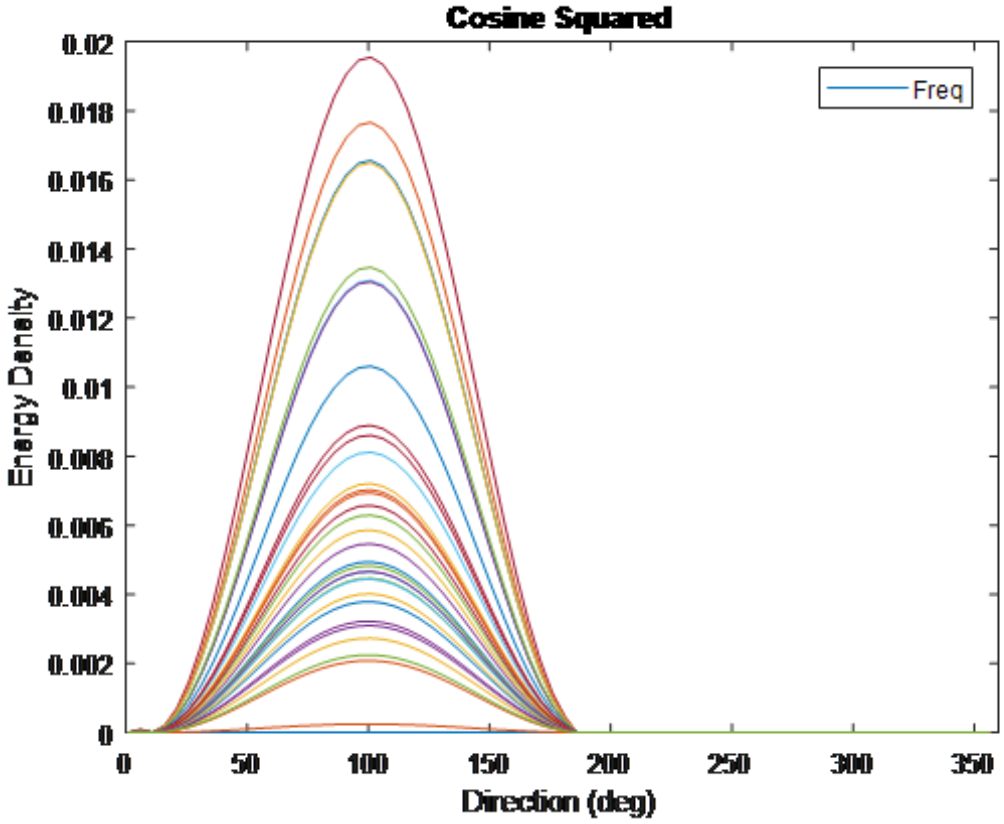

Figure A.6 Cosine squared distribution

Cosine 2s is similar to the cosine squared function but utilizes a spreading parameter "s". This changes the expression to:

$$D(f,\theta) = G(s)\cos^{2s}(\frac{\theta-\theta_m}{2}) \qquad \text{(A.15)}$$

Where, $(s) = 0.5\sqrt{\pi} * \frac{\Gamma(s+1)}{\Gamma(s+0.5)}$, $s = \frac{r_1}{1-r_1}$, , and r_1 is the first Fast Fourier

Transformation coefficient.

The addition of the "s" parameter produces a different cosine squared shape (figure A.7).

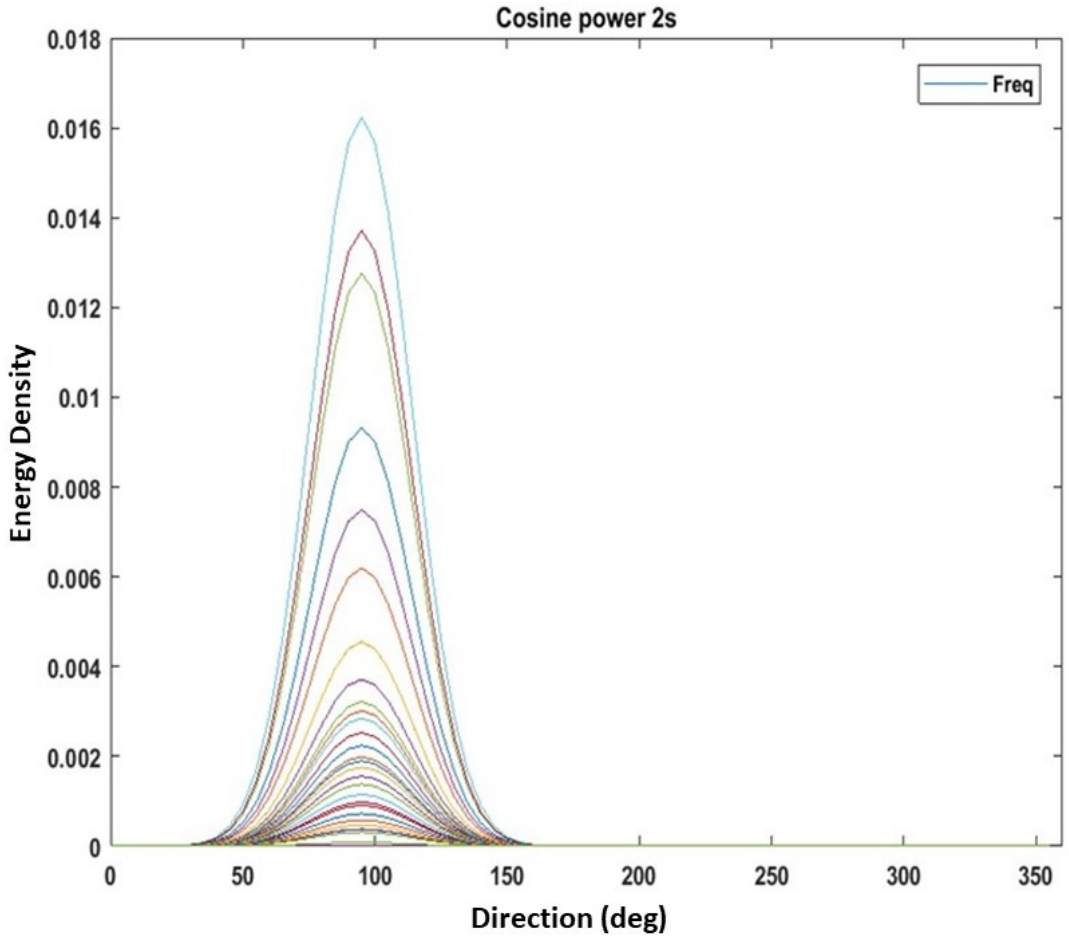

Figure A.7 Cosine 2s distribution

A.4 Nearshore Wave Models

Models have become an integral part of the coastal engineering process. The purpose of nearshore wave transformation models is to simulate the multiple processes that occur as a wave moves from deep water to shallow water (Smith, 2001). Nearshore wave models are based on the conservation of wave momentum and wave energy. There are two main types of nearshore wave models: phase-resolving and phase-averaging. Phase resolving models are based on the mild slope equation (Demirbilek and Panchange

1998), or Boussinesq equations (Nwogu and Demirbilek, 2001). These models have the ability to resolve changes in wave properties that occur on the subwavelength scale, or the physical processes such as reflection and diffraction (Rusu 2009). Therefore, if detailed reflection and diffraction patterns are needed, then a phase resolving model would be the most appropriate choice (Kaihatu et al. 1998). Alternatively, phase averaging models are models based on the wave action balance equation (Holthuijsen 2007). The wave action balance equation was introduced by Bretherton and Garrett (1970) and is defined as the energy density, or the extractable energy stored in a system per unit volume, divided by the relative frequency (Goncalves et al. 2012). Phase averaging means that all the phases are considered to be random and no phase information is tracked (Smith 2001). This means in a phase averaging model only propagation towards shore is considered with no reflection. The third-generation phase averaging models are currently the most state of the art. SWAN (Booij et al. 1999, Ris et al. 1999), the first third-generation spectral wave model, and STWAVE (Smith et al. 2001) are two current phase averaging models explicitly designed for nearshore applications (Van der Westhuysen 2012).

Both SWAN and STWAVE models have been extensively studied, validated, and compared. Siadatmousavi et al. (2016) looked at the sensitivity of SWAN to wind and boundary condition sources. Goncalves et al. (2012), Kaihatu et al. (1998), Rusu et al. (2011), and Slinn (2008) all compared STWAVE and SWAN by performing sensitivity analyses. Goncalves et al. (2012) gave the most extensive review and concluded that the choice of use between the two nearshore wave models is entirely dependent upon the user's preference for computational efficiency, the user's available computing power, the

area of interest, and the intended goal of use for the model, as statistically the two performed similarly (Goncalves et al. 2012). For use in this study, STWAVE was chosen because of the uniform bathymetry, the mild environment and the interest in propagation only towards shore. STWAVE was also chosen for its faster computational efficiency.

A.4.1 STWAVE

STWAVE is a stationary, finite differencing, phase averaging, spectral wave model based on the wave action balance equation, which is able to quantitatively describe changes that are due to the influence of bathymetry, currents, and water level on wave parameters as a wave moves towards shore. STWAVE simulates wave-bottom interactions, the influence of currents, refraction, shoaling, and breaking and the corresponding changes to wave energy. STWAVE is run on a Cartesian grid, with the x-axis in the cross-shore direction and the y-axis in the alongshore direction. The offshore boundary is set parallel to the shoreline. The units of the model are metric with water heights and depths all in meters. Wind speeds are reported in meters per second, wave periods in seconds and energy densities in m2/Hz/radian. Wave and wind direction are input and output in units of degrees measured counterclockwise from the grid x-axis, however, within the model computations they are converted to radians (Massey et al. 2011).

The model can be run solely off the .sim file, which is a FORTRAN namelist file containing the chosen model controls. However, optional inputs include a bathymetry grid, a directional wave spectrum, and wind speeds (Smith, 2007; Smith, 2001). The model then uses these inputs to transform the waves as they travel inshore and outputs the

wave parameters of height, peak wave period, and mean wave direction at all grid points and also outputs two-dimensional spectra at selected grid points (Smith, 2001).

STWAVE computes wave transformation in two modes: half plane and full plane. The differences between the two modes are how they treat wave direction. The half plane mode spreads wave energy at + 85-degrees from the x-axis offshore and ignores any energy traveling in a negative x-axis direction (i.e. reflection). While, the full plane mode allows wave energy to spread over 360-degrees. The benefits of half plane mode versus full plane mode is that even though it is limited in direction resolution, it is computationally faster, requires less memory, and for most applications, except semi-enclosed bays and lakes, it is functionally appropriate. The half plane mode is not appropriate in semi-enclosed bays and lakes because there is not an obvious offshore location to start the wave transformation. The half plane mode divides the 170- degrees on its boundary into 5-degree bins, and also requires the grid spaces to be equal. There are two ways to execute both modes: serial and parallel. For this study, parallel execution using the half plane mode was chosen for efficient computation, the open boundary location, and the interest in propagation only.